5-2020

DMD and POD Modal Analysis for Store Separation

Nicholas Peters

DMD AND POD MODAL ANALYSIS FOR STORE SEPARATION

By

Nicholas Peters

A Thesis Submitted to the Faculty of Embry-Riddle Aeronautical University

In Partial Fulfillment of the Requirements for the Degree of

Master of Science in Aerospace Engineering

May 2020

Embry-Riddle Aeronautical University

Daytona Beach, Florida

DMD AND POD MODAL ANALYSIS FOR STORE SEPARATION

By

Nicholas Peters

This Thesis was prepared under the direction of the candidate's Thesis Committee Chair, Dr. John Ekaterinaris, Department of Aerospace Engineering, and has been approved by the members of the Thesis Committee. It was submitted to the Office of the Senior Vice President for Academic Affairs and Provost, and was accepted in the partial fulfillment of the requirements for the Degree of Master of Science in Aerospace Engineering.

THESIS COMMITTEE

Chairman, Dr. John Ekaterinaris

Reda Mankbadi Digitally signed by Reda Mankbadi Date: 2020.04.27 09:21:26 -04'00'

Member, Dr. Reda Mankbadi

Richard J. Prazenica Digitally signed by Richard J. Prazenica Date: 2020.04.28 20:48:24 -04'00'

Member, Dr. Richard Prazenica

Dr. Magdy S. Attia Digitally signed by Dr. Magdy S. Attia Date: 2020.04.29 10:59:58 -04'00'

Graduate Program Coordinator, Dr. Magdy Attia

4/29/2020

Date

Dean of the College of Engineering, Dr. Maj Mirmirani

5/5/2020

Date

Christopher Grant

Associate Provost of Academic Support, Dr. Christopher Grant

5/6/2020

Date

ACKNOWLEDGMENTS

Before proceeding any further I need to acknowledge my family and loved ones for their love and support though out my college education. If it was not for them I would have neither the motivation nor ability to pursue a higher education. Their support over the years has come through actions as large as offering advice in life changing decisions to simply showing an interest in my work as I've strived to complete my education.

I would like to specifically acknowledge my mother and father for always supporting me and never faulting in their constant love. Even when mistakes were made and I seemed to be heading down wrong paths they have always showed an unwavering support. They have been incredible role models to me.

I would also like to acknowledge my brother and sister, Anthony and Cara. Growing up along side both of them has made me the person I am today. Their competitive nature and strong fortitude has left a lasting impact on me.

This thesis would also not have been completed if it were not for the support of my girlfriend, Tamara Chambers. She has help support my decisions from before I even selected which graduate school I would apply to. Having such a close friend is something I am truly grateful for.

I also need to thank Elias Wilson for listening to me complain about problems with my thesis, which often times resulted in a solution for my thesis. We have both know each other since undergraduate and having a friend who is as motivated as Elias and going through the same education route is something I'm very thankful for. Additionally, thanks to Nicholas Zhu for fixing my office chair.

This thesis would not have made the progress it's made without the assistance of the committee members, Dr. Prazenica and Dr. Mankbadi. The assistance of Dr. Prazenica and his graduate students has been extremely valuable to this work. In addition, the many office visits with Dr. Mankbadi and many classes I have taken with him has been more of a help than I can say.

Lastly, I would also like to make a special acknowledgment of the help I have

received from my graduate advisor, Dr. John Ekaterinaris. If I were to list all the help Dr. Ekaterinaris has provided me in just the past two years the list would extend another three plus pages. There are summer internship opportunities, research topics, and conferences I would ever have been exposed to if it were not for my advisor. Thank you for doing so much to help my career and for making my graduate studies such an enjoyable experience.

ABSTRACT

Store separation from aircraft and spacecraft has historically been a critical and in some cases fatal issue for the aerospace industry. Given the severity of the issue much effort has been spent on the development of processes to identify failure flight conditions for store separation. The processes currently used for identifying potential failure conditions however are both resource intensive and iterative processes. A potential remedy to reducing resource use and improve turn around time in this process is the implementation of a mode based reduced order model (ROM) for modeling store separation. The objective of this study was to first identify the leading modes that can best be used to model a store separating from an aircraft. To obtain these modes, two algorithms were used; Proper Orthogonal Decomposition (POD) and Dynamic Mode Decomposition (DMD). The computational fluid dynamic (CFD) solver Ansys Fluent was employed to obtain flow field data around a representative vehicle and store. Preliminary validation of the numerical results was initially preformed and the results showed good comparison of surface pressures and free-stream vorticity. The validated data-set was then used to identify which modal method, POD or DMD, better resolves the known dominate structures of the flow field. The results of this analysis showed the superiority of POD in identifying both free-stream and surface pressure structures. A final representative case of store separation was obtained at a flight speed of mach 0.8. POD was then used to obtain leading modes that were used to reconstruct a ROM of the flow field. This ROM was successful in predicting the store's trajectory both inside and out of the training flight profile.

TABLE OF CONTENTS

LIST OF FIGURES

Figure Page

Figure Page

Figure Page

Figure Page

LIST OF TABLES

NOMENCLATURE

α	angle of attack
α'_k	a vector of k constants
λ	eigen values
μ	dynamic viscosity
ν	kinematic viscosity
ω	eigen vector
Φ	modes
ρ	density
ρ_∞	free stream density
Σ	eigen values for modes
σ	singular values percentage
τ	shear stress
A	time correlation matrix
a_t	reconstructing time coefficients
A_{cell}	surface area of cell face
C	correlation matrix
e	specific energy
F	force
I	moment of inertia
KE	kinetic energy
L	length scale
M	moment
P	pressure
q	heat rate
q	pitch rate
t	time
T_∞	free stream temperature

U	mode matrix
u	a vector of velocity
u_0	mean velocity
U_∞	free stream velocity
u_x	first DMD snapshot matrix
u_y	second DMD snapshot matrix
V^T	SVD matrix containing time information
X	snapshot matrix
x	a vector if p random variables
x	x-position
X_0	mean of snapshot matrix X
X_P	pertubated version of snapshot matrix X

1. Introduction

The first question that might arise from reviewing this study's abstract is simply: what is store separation? Often an overlooked topic in aviation, store separation simply refers to the task of releasing one body from another in flight. Perhaps the most intuitive and seemingly elementary example of this is the releasing of an external fuel tank mid-mission. The topic of store separation expands drastically from here. Examples are numerous including the releasing of cavity missiles from stealth fighters at supersonic speeds, separation of booster rockets from space shuttles, ejection of torpedoes from submarines, etc..

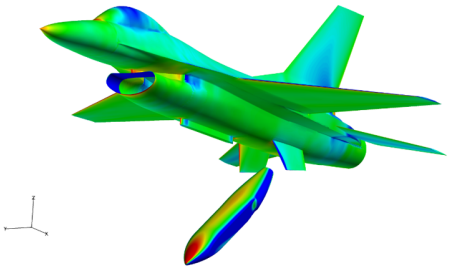

Figure 1.1 Example of store separation (Israeli Computational Fluid Dynamics Center, 2010).

The next question to arise could potentially be: how challenging is the task of store separation? While from a surface level observation the task of store separation appears relatively benign, a closer observation unveils an almost unanticipated level of complexity. Take the example of simply releasing a fuel tank from a military aircraft. This might appear to be a simple case: nonetheless there is a high level of complexity to this example.

Let us first isolate the aircraft. At high velocities as the flow moves along the length of the aircraft, a significant turbulent boundary layer begins to form. This boundary layer can in some cases contain turbulent structures which can often make separation difficult. In addition, the store itself is also building its own equally complicated boundary layer. It is difficult to predict the flight conditions for which the combined effect of these turbulent boundary layers can be so great that a store will fail to smoothly break free. In mild cases,

the store will have an erratic unpredictable trajectory. In the most extreme of cases, the store can in fact be sucked back into the vehicle, resulting in the complete destruction of the aircraft.

1.1. Store Separation Failure

Typically, these cases of failure to separate can be narrowed down to three potential cases. In case one, there is an attempt to release multiple stores at once. In many cases, the combined aerodynamic interaction of multiple stores causes complicated wake store interactions, which leads to an extremely difficult to predict trajectory of the stores. While this is potentially a case of high interest, due to its aerodynamic complexity it will not be pursued in this study. The computational power and time required to analyze such cases is beyond the time frame allowed for this study.

In case two, a single store is released from an aircraft. During the separation, the store's trajectory is altered by the aerodynamic influence of the fuselage's boundary layer. In these cases, the store follows an erratic path making precision targeting non-feasible.

In the third case, a single store is again separated from the aircraft. In this case, the store becomes unstable once isolated from the aircraft. This is a result of an initial perturbation influenced by the aircraft's boundary layer. In this situation, rather then being dominated by store-fuselage aerodynamic interactions, a failure to separate is dominated by isolated stability characteristics of the store itself. This case is potentially the most dangerous as the store can often collide with the aircraft at very high speeds, causing significant damage. Cases two and three of a failed release of the store will be the main focus of the study and as such the mechanisms of separation failure related to fuselage-store interactions and an isolated store will be investigated.

The flight conditions which have most often led to failed store separation conditions are associated with transonic and supersonic speeds. Generally speaking, at low speeds the concern of safely releasing a device from an aircraft is relatively low as the mass of the store generally can simply outweigh any aerodynamic loads that might be experienced. This explains why pilots during the First World War would often simply

toss munitions from the cockpit down onto enemy positions. For these low speed aircraft, the store separation analysis was limited to simply testing a pilot's arm strength. Yet as the maximum velocities of military aircraft began to increase drastically both during the Second World War and after the advent of the jet engine, the ability to safely separate these stores became an issue which required much more attention.

Figure 1.2 A crew member of a British SS 'Z' Class airship about to throw a bomb from the rear cockpit of the gondola (Imperial War Museums, 2014).

1.2. Trajectory Prediction Methods

In this subsection of the Introduction, the various methods currently used to study store separation will be reviewed. Each of these methods have their own advantages and disadvantages of which it is important to have a surface level understanding before grasping both the objective of this work and its importance. Without understanding the capabilities and limitations of the current store separation analysis methods, it will be difficult to understand the need for and importance of constructing a reduced order model (ROM).

As previously mentioned, the desire to truly begin investigating store separation began after the Second World War in the early 1950s. Given the nearly complete lack of computational power and limited experimental capabilities, the initial store separation analysis was completed using a simple 'Hit or Miss' strategy (Cenko, 2010). In this

strategy, a specific store would be released from an aircraft at increasing velocities until it was deemed too dangerous to continue. While this method may seem crude, the 'Hit or Miss' strategy still remains to this day the quickest method for identifying the dynamics of separation. This 'Hit or Miss' method has been used as recently as Operation Iraqi Freedom in which the United States Navy quickly needed to include an external fuel tank to increase the range of their F-18C fighters. Given the immediate need to get the fuel tank cleared for flight and the fact that the Navy had neither an experimental or computational model available for analysis, it was decided that this 'Hit or Miss' method would be used. Yet, despite its efficiency in clearing stores for flight in a timely manner, the 'Hit or Miss' method is still highly dangerous and has resulted in the destruction of many test aircraft over the years (Cenko et al., 1996).

It wasn't until the 1960s that a new method was developed for the store separation analysis. This method was called the Captive Trajectory System (CTS) (National Aerospace Laboratories, 2018). In this method, a store, using a lever arm, is released from a scaled down model aircraft in a wind tunnel. During the separation, the lever arm creates a log of the forces and moments experienced by the store. These forces and moments can then be used to build a 6-degree of freedom (6-DOF) model to predict the trajectories of the stores. While this method greatly increases the safety of the analysis, it also can become an extremely time consuming and expensive process. Additionally, as with many wind tunnel experiments, difficulty arises in this method from concerns over scale corrections to the flow. Often, it is the boundary layer around the aircraft which leads to a failed separation. This boundary layer can be extremely difficult to accurately reproduce around the aircraft to the proper scale and takes much time and care to do so. Additional difficulties include acquiring the highly specialized equipment required for a CTS experiment and running dozens of experiments to capture the many flight conditions with a wide range of potential store configurations (Cho, Kang, Jang, Lee, & Kim, 2010).

Given the great expense associated with CTS, there has long been a desire to find an alternative way of clearing stores for flight. As the computational power available

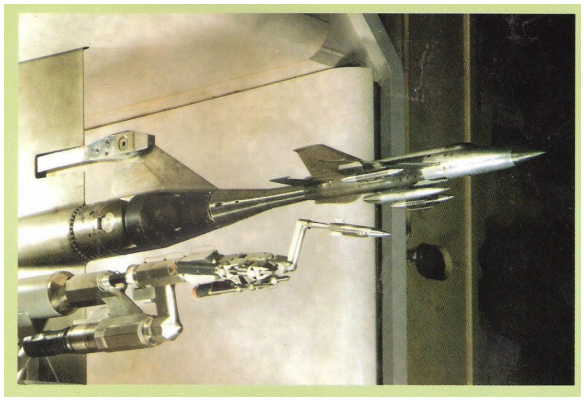

Figure 1.3 CTS (National Aerospace Laboratories, 2018).

to engineers began to expand exponentially in the 1970s, many engineers looked to computational fluid dynamics (CFD) as a cheap alternative to wind tunnel experiments. One of the first applications of CFD to store separation was through the use of panel methods. Panel method codes rely on the use of summation of elementary flows (i.e. vortex, sink, source, doublet) to form a full flow field around a body. At first, these codes struggled to analyze a single store separation flight condition in under 24 hours. Yet, given the explosion in computational power available to engineers since the 1970s, panel codes have proven to be a capable tool in efficiently analyzing low Reynolds number and minimal flow separation cases (Cenko & Tinoco, 1979). Codes such as USAERO and Tornado have be used extensively to provide trajectory predictions throughout the years.

The two greatest advantages which have allowed panel codes to achieve such success in this area is their speed in running cases and their robustness in dealing with complex geometries. The store separation analysis requires the ability to examine tens, if not, hundreds of flight conditions for various possible configurations of an aircraft. The panel code algorithm allows for a simple matrix inversion of a relatively small matrix to obtain a quick solution at each iteration in the simulation. This simple matrix inversion leads to the second advantage to panel methods, robustness. Since there is no need for the incorporation of finite difference/volume methods, this eliminates the need to worry about convergence issues. Yet, panel method codes still have their disadvantages. By remembering that these methods only use elementary flows, it is intuitively realized

that there is a lack of ability to grow turbulent boundary layers (aside from boundary layer corrections) and model highly separated regimes of flow. So despite these great advantages panel codes are still greatly limited in their application to the topic of store separation.

All hope is not lost, however, for CFD calculations to take a larger role in the store separation analysis. As computational power has continued to grow ten fold every five years, there has been a new potential for CFD applications (Zikanov, 2019). For high Reynolds number/highly separated flows engineers have for the past twenty to thirty years attempted to use Unsteady Reynolds Averaged Navier-Stokes (URANS) CFD simulations to safely identify potentially dangerous separation scenarios (Panagiotopoulos & Kyparissis, 2010). While URANS has been highly successful in analyzing specific flight conditions, technology has not progressed to a point where run times are fast enough to efficiently complete store separation analysis across an entire flight profile.

This leads to the critical challenge facing the aviation community today. We have a method, through URANS, to obtain a good representation for the flow field during store separation. Yet despite the fact that we now have hundreds, or even thousands, of computer processors available for parallel computing, simulation times using URANS still require multiple days for each flight condition. The issue of incorporating turbulence modeling simulations into the preliminary design analysis has been a dominant issue across multiple industries. Through the work of multiple groups across these industries, it has been realized that often fluid flows which posses thousands, if not millions, of degrees of freedom can be dominated by orders of magnitude fewer degrees of freedom. This has led to the desire of obtaining a reduced order model (ROM) which can somehow incorporate only these leading degrees of freedom of the flow field to make a simulation capable of running orders of magnitude faster than URANS while still maintaining a high degree of accuracy. Yet there remains many unknowns in this process of constructing a ROM such as obtaining dominant fluid structures.

The identification of these fluid structures will be the first objective of this study.

In essence, this objective is to use two of the leading methods for identifying fluid structures, Proper Orthogonal Decomposition (POD) and Dynamic Mode Decomposition (DMD), to identify the capabilities of these methods to obtain leading fluid structures (modes) which can then be used to reconstruct the original system. The second objective will then be to apply this modal subspace to reconstruct a ROM which will then be used to model store separation from the aircraft at a fixed flight condition. These objectives aim to provide the field with a fast method for identifying an appropriate modal subspace and a proof of concept that this subspace can be used to construct a ROM which operates at low computational cost while still retaining a high degree of accuracy.

1.3. Summary of Simulations

The CFD simulations which were used in this study will be now summarized. The first step for this study was to define a model for the store. After a literature review, it was decided to use a 6:1 prolate spheriod. This body was chose for two reasons. First, the body serves as a good representation for a large array of stores. A 6:1 prolate spheriod draws a good representation to both an external fuel tank and an unpowered bomb, objects of great interest in the store separation topic. Second, the 6:1 prolate spheriod is a body which has had numerous well documented and reviewed experimental studies. As with any computational model, before the study could progress it was essential that there be a comparison to experimentation. For this study, the experiments used for validation came from a series of studies completed by Wetzel in 1996 at Virginia Tech University (Wetzel, 1998). The studies completed by Wetzel include measurements for both steady-state and transient results and will be examined further in the Overview of Experiment section of this thesis.

The first series of simulations which were completed in this study were all done using steady-state assumptions. In these simulations, the store's body had a length of 1.372 m and was placed in sea level conditions with velocity of 45.7 m/s. The store was then held at a fixed pitch of 20 degrees. With the operating conditions fixed, the study used multiple combinations of grids and turbulence models to identify the most

computationally efficient method for modeling the store. In total 9 cases were examined.

After the steady-state cases were completed, two pitch up motion simulations were run from 0 to 30 degrees pitch at a fixed pitch rate of 90 degrees per second. The same operating conditions were used as in the steady-state simulation. A comparison was then drawn to experimentation to validate the model. In addition to model validation, these transient results were used to identify which modal method, POD or DMD, would best resolve the known experimentally determined fluid structures.

Once the simulation model was validated and a modal method was selected, a single transient simulation for store separation was completed. For reasons which will be explained in the following subsection 'Scope and Limitations', it was decided that the representation for the fuselage in this simulation would be the 6:1 prolate spheriod. This fuselage was fixed at 1.372 m. The store was then taken to be .343 m or one quarter the size of the original size of the store which was validated. The mass of the store was fixed at 10 lbs. This store was then placed at .05 m displacement from the surface of the fuselage and released at a mach number of 0.8. The results from these simulations was then used with the selected modal analysis algorithm to first identify a subspace for store separation. The study then constructed a ROM for store separation based on this subspace.

1.4. Scope and Limitations

As in any study this investigation had a series of limitations. The first of these limitations came down to computational power and time available to complete the project. The study was extremely fortunate to have access to the Embry-Riddle Aeronautical University's (ERAU) Vega Super Cluster Super Computer. Without access to the 360 2.3GHz CPUs available per graduate student, the work completed in this study would not be possible. Yet, even with this large computational power available the study was not unlimited in its resources. In this study, the average cell count was often found to be between 8-15 million cells. Additionally, to model the proper fluid structures required in the transient simulations time steps as small as 1e-5 seconds were used.

The combination of these factors led to significant run times for transient simulations, often needing between 5-7 days for each case. Given this large run time, much care was needed to limit complexity whenever possible in the simulations to ensure both accurate physics were being captured and total time between simulations was minimized. For these reasons, when selecting the fuselage for the store separation trials it was decided that the same 6:1 prolate spheriod as from the validation study would be used. This selection has the significant advantage of providing the study with not only simple but accurate representations for a generalized fuselage body, but also meant there would be no additional requirement to validate the model for the fuselage.

An additional limitation of the study was access to experimental data. As mentioned in the Trajectory Prediction Method subsection of the Introduction, experimental analysis of store separation is an extremely time consuming and resource intensive task. Much of the experimental data available for store-fuselage/store-store interactions or complex geometries, such as through CTS, are currently held by private corporations and not available to the public. As such, the study was limited to a very general shape. Additionally, the experimental results which were available, while well documented, did not account for body-body interactions. As such, a validation for store-fuselage/store-store interactions would not be possible.

1.5. Organization of Paper

This thesis will be organized as follows. After the Introduction, a literature review will be presented. In this section, the current state of the mode identification and mode-based-ROM construction will be reviewed. Next, a Modal Analysis section will be presented. In this section the bases for POD and DMD will be explained. Their respective algorithms will be reviewed along with any inherent advantages or disadvantages associated with them. In the next section the exact experiments completed by Wetzel will be reviewed in more depth. Both the experimental setup and final results used for comparison will be presented.

The CFD simulation case setup will be discussed in the proceeding section. In this

discussion, the turbulence models selected in this study will be reviewed in addition to the numerical schemes used. The generation of grids for all cases are also summarized here. As a final step for this section, the 3-degree-of-freedom (3-DOF) model created by this study will be reviewed.

From here, all results obtained in this study will be analyzed and discussed. These results are first grouped as simulation or ROM results. From here they are further decomposed into pitch up or store separation cases.

A final section is presented with the objective of outlining the conclusions of the study. Additionally, future work building off of the study will be discussed.

2. Literature Review

The main two objectives of this study are to first identify leading modes for store separation and second, use these leading modes to construct a mode-based ROM. As such, a literature review is reviewed to review relevant work in the field. This literature review will be broken down into two sections, one where modes are identified and another where the modes are used for a ROM.

2.1. Mode identification

Mode identification has been a topic of interest in a wide range of diverse fields for several decades. This interest has been driven by the realization that very large data-sets containing numerous degrees of freedom can often be defined by an extremely low dimensional subspace. In other words, large data-sets can often be compressed into an extremely small amount of data while still maintaining the original information. This characteristic was first discovered in 1901 through the work of Karl Pearson. Pearson (1901) developed the algorithm for Principle Component Analysis (PCA). PCA, Equation 1, is essentially a method for identifying representative subsets of data (modes) which dominate the original data-set. In Equation 1, x is a vector of p random variables and α_k is a vector of k constants.

$$\alpha_k' x = \Sigma_{j=1}^{p} \alpha_{kj} x_j \tag{1}$$

It was through this algorithm that the basis of modal analysis was later developed and reformulated for numerous fields. The first application of modal analysis to turbulence was initially introduced in Lumley (1981). In this study, Lumley showed how a modal analysis could be successfully used to identify coherent turbulent structures in the flow field. Since then, various studies have incorporated some form of modal analysis for understanding the fluid dynamics of a system. A more in-depth review of the history of mode identification in regards to POD and DMD will be presented in the Modal Analysis section of this thesis.

Often, the objective of these works are centered on attempting to identify underlying

flow structures of a recorded domain. In one such study completed by Iqbal in 2007, POD was used to investigate coherent structures coming from an axial-symmetric turbulent jet (Iqbal & Thomas, 2007). All of the data used in Iqbal's study were obtained experimentally.

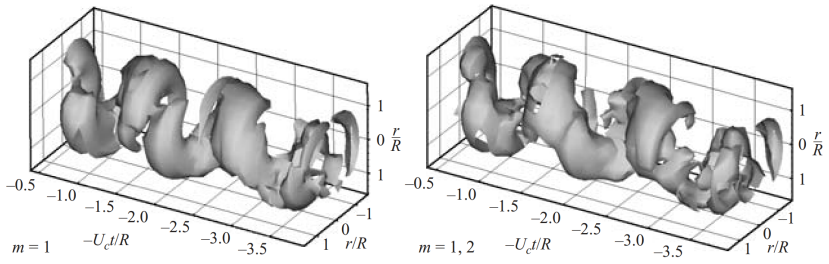

Figure 2.1 The projection of the first POD mode,(u, w)-components (Iqbal & Thomas, 2007).

In a separate experiment completed by Lengani et al. (2017), both DMD and POD were used to help analyze the laminar separation bubble found in ultrahigh-lift low-pressure turbine blades. The objective was to identify the process by which the laminar separation was occurring on the turbine blades through a modal analysis. Leading modes were found from slices of the flow field obtained through Particle Image Velocimetry (PIV) measurements. This information was then used to identify possible ways of reducing the laminar separation bubble.

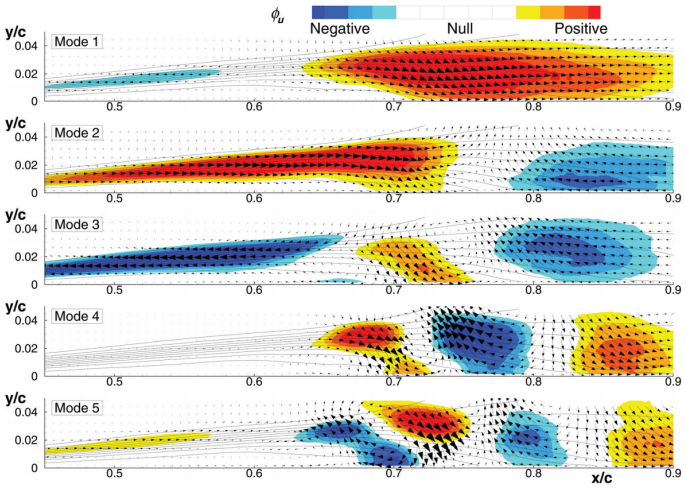

Figure 2.2 POD modes of the streamwise velocity component and their vectorial representation (Lengani et al., 2017).

Numerous other examples can be found in the literature of groups attempting to

identify modes in fluid dynamics. Some of the methods used in a typical modal analysis along with their advantages and disadvantages will be discussed in the Modal Analysis section of this thesis.

2.2. Reduced Order Model

Just as there have been numerous studies focused on analyzing fluid flows through modal decomposition, there have been a similar number of studies focused on how best to leverage these modes into a ROM. These studies tend to fall into two main categories, interpolation models and governing equation reduction modeling.

The simplest of the interpolation models is where studies will simply project the found modes back onto the original data-set with the objective of seeing how well a limited number of modes represent the original system. An example of this methodology can be found in a study completed by Liberge and Hamdouni (2010). In this study, an oscillating cylinder was modeled using CFD. The data-set was then organized into a snapshot matrix which was then analyzed using POD. Liberge and Hamdouni then reduced this mode set down to as few modes as possible while still attempting to retain as much of the original data's information as possible. As a final step, the selected subset of modes were projected back onto the original data-set and a comparison was made to see if the Von Karman vortices still appeared correctly. The results of this study showed that with only retaining 6 modes, the Von Karman vortices could be retained with a high degree of accuracy.

Another methodology used to construct mode-based ROM's is through an interpolation of time coefficients. These time coefficients will be discussed in more detail in the Modal Analysis section of this thesis. The main objective of this interpolation method is to construct a function for the time coefficients which is based on a limited number of inputs. A major question to arise in using this modeling method is how will these interpolations be made. The methodology used to construct these interpolations can usually be classified into two main approaches. The first is a simple least squares regression and the other methodology used is called Kriging interpolation. Both of these

methods are based on fitting a function to an under determined system. An example of a study using Kriging interpolation can be found in a study completed by Mohammadi and Raisee (2019). In this study, a method was proposed for developing a data-driven ROM capable of analyzing turbulent channel flow simulations. This study found that with only 6 modes, an extremely accurate comparison could be made between the ROM and full order simulation when comparing Nusselt numbers (Figure 2.3).

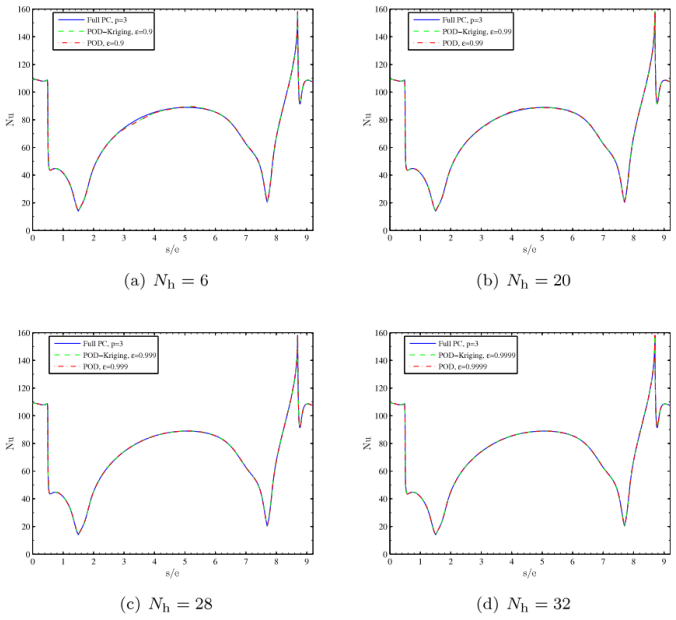

(a) $N_h = 6$ (b) $N_h = 20$

(c) $N_h = 28$ (d) $N_h = 32$

Figure 2.3 Comparison between mean values of Nusselt number obtained using POD and POD–Kriging methods with various high-fidelity samples (Mohammadi & Raisee, 2019).

A final, and possibly most computationally expensive, technique used to construct a ROM using modes is to use a projection-based ROM for the Navier-Stokes equations. To model the evolution of the velocity field the process starts with the incompressible Newtonian fluid.

$$\nabla u = 0 \tag{2}$$

$$\frac{\partial u}{\partial t} = \nu \Delta u - \nabla(uu) - \nabla P \tag{3}$$

The standard projection-based MOR apporach is then applied using the spatial basis

functions found using POD (Noack, Morzynski, & Tadmor, 2011).

$$u(x,t) = u_0 + \sum_{i=1}^{n} a_i(t) u_i(x) \tag{4}$$

In Equation 4, $u_i(x)$ are the spatial basis functions found using POD, u_0 is the stationary mean flow pattern, and $a_i(t)$ are the reconstructing time coefficients. From here, the Galerkin projection of this basis set is taken for the Navier-Stokes equations. The projection yields the below ordinary differential equations in canonical form.

$$\dot{a}_i = \sum_{i=jk}^{n} Q_{ijk} a_j a_k + \sum_{i=j}^{n} D_{ij} a_j + b_i \tag{5}$$

For divergence free spatial basis functions with steady dirichlet boundary conditions, the below Galerkin matrices are formed.

$$Q_{ijk} =< u_i, \nabla(u_j u_k) >_\Omega \tag{6}$$

$$D_{ij} =< u_i, \nu\Delta u_j - \nabla(u_0 u_j) - \nabla(u_j u_0) >_\Omega \tag{7}$$

$$b_i =< u_i, \nu\Delta u_0 - \nabla(u_0 u_0) >_\Omega \tag{8}$$

Note that the matrices Q_{ijk}, D_{ij}, and b_i are computed at each time step where u_0 is the first mode found in the POD algorithm. It is also important to note that this ROM formulation only works for flow velocity. This form of a ROM is simply introduced in this section so the reader is aware of all types of ROM used in academia.

3. Modal Analysis

In this section, the two methods used to identify the leading modes of the system will be reviewed. In this review, the algorithm for these two methods will first be presented. Following this discussion, the various advantages and disadvantages of the two modal analysis methods will be presented. However, before any discussion on these methods can continue, some background information is necessary.

3.1. Snapshot Matrix

First, it must be covered as to what a snapshot matrix is and how to construct one. Consider the example of having completed a transient simulation using a CFD solver. At a specified time interval, 'snapshots' are taken of the flow field. These snapshots simply provide the instantaneous solution for the flow field at set intervals of time. Once a sufficient number of snapshots are obtained, a matrix can be formed as follows. First, for each snapshot select a scalar value to analyze. Second, align all the element values into a single row for each snapshot. For example, if the computational domain uses m cells then the total number of rows for each snapshot array will be m. Last, combine all the snapshot arrays into a single snapshot matrix. For example, if the computational domain uses m cells and there are n snapshots, then the snapshot matrix will be m-by-n.

While the premise behind a snapshot matrix is relatively simple, much care needs to be made in constructing this matrix as this will influence the effectiveness of the POD and DMD algorithms. Keep in mind that the objective is to obtain the leading structures that appear in the flow field. As such, it is essential to have a significant series of snapshots so that all of the structures that define the physical system are captured. For instance, if a large time step is used and only five snapshots of the flow behind a cylinder are used then much of the information for the spatial correlations as they appear in the flow will be missed. This means that any structures that appear in the flow field at low frequencies and high growth rates will fail to appear during the modal analysis algorithms. Furthermore, if there are a large number of snapshots but the time spacing is larger than the vortex shedding frequency, then many of the temporal correlations that are present will be

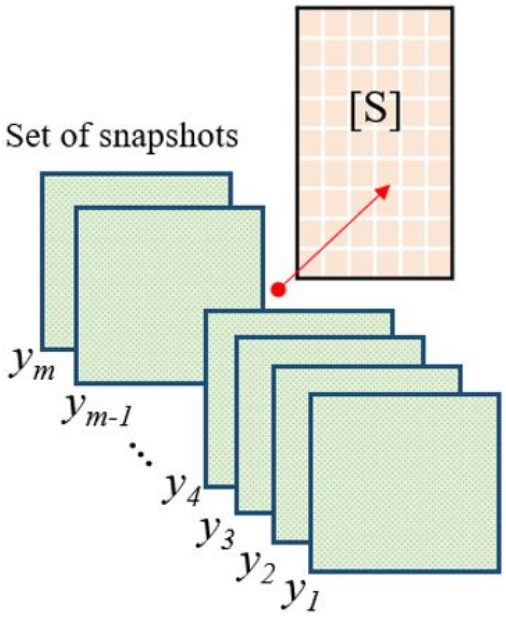

Figure 3.1 Snapshot matrix (Paul & Chang, 2017).

missed. This means that any structures of the flow field that appear at fixed frequencies will be missed. A general rule for resolving temporal correlations is to first identify the period associated with the flow field. Then, attempt to obtain 10-50 snapshots per period. This snapshot per period number will vary greatly depending on how many periods are present in the data-set. If, for example, there is only 1 period in the data-set, the snapshots per period will be much larger than 10. Yet, if the number of periods are closer to a hundred, it is possible to resolve temporal correlations with fewer than 10 snapshots per period.

In essence, a snapshot matrix is a matrix representation of any given system whether it be from simulation or experiment. This matrix representation can contain orders of hundreds of thousands or even millions of degrees of freedom, and it is the objective of modal analysis algorithms to reduce the number of states in this system as much as possible while still maintaining the physics of the full-state system.

3.2. Single Value Decomposition

The second important background knowledge to have going into this analysis is on Single Value Decomposition (SVD). SVD is a matrix decomposition method

which is guaranteed not only to exist but be stable for every matrix. In this method, there is an attempt to decompose the targeted data-set into its most dominant statistical structures. Through this decomposition, a subspace is found which allows for an accurate representation of the original matrix. It is for this reason that SVD has historically greatly been used for image compression. Given the large success of SVD in this application, it has since been applied to numerous other topics such as electric signal processing, MRI data processing, internet search engine algorithms, and fluid dynamics. Possibly the most remarkable aspect of this statement is that across multiple disciplines large data-sets which typically contain a large number of degrees of freedom are dominated by a relatively low-dimensional subspace.

The starting point the SVD analysis is a snapshot matrix composed of n snapshots:

$$X = [x_{t_1}, x_{t_2}, ..., x_{t_n}] \tag{9}$$

Through SVD *X* can be decomposed into a series of matrices.

$$X = U\Sigma V^T \tag{10}$$

U and *V* are both square matrices which have orthonormal columns. The dimensions of *U* are identical to *X*'s row dimension while the dimensions of *V* are determined by *X*'s column dimension. The Σ matrix is then a diagonal matrix containing the singular values of the *X* matrix ordered from largest to smallest. These singular values are often defined as representing how much information of the full data-set is contained in each column of the *U* matrix. By selecting a reduced rank *r* for these matrices and taking their product, a reduced representation for the original data-set can be formed. Often, the objective in data reduction is to select the optimal *r* to satisfy Equation 12. Figure 3.2 provides a good representation as to how data-sets, in this case the image of a dog, can be reduced significantly while still retaining much of the original information.

$$\hat{X}_r = \hat{U}_r\hat{\Sigma}_r\hat{V}_r^T \tag{11}$$

$$min[|X - \hat{X}_r|] \tag{12}$$

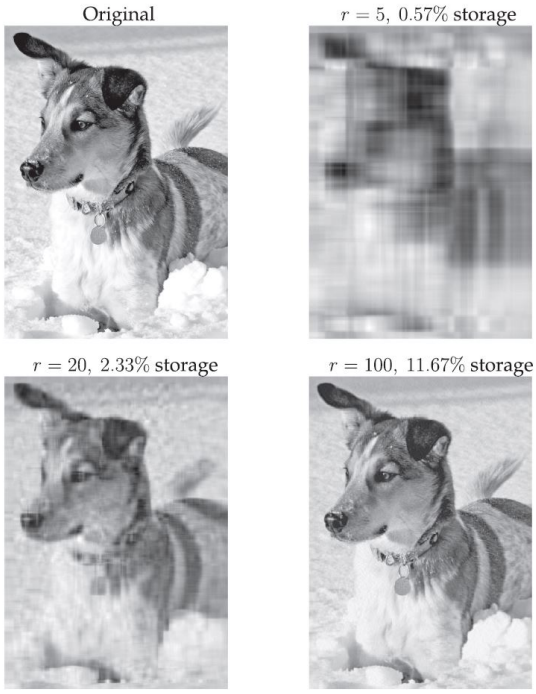

Figure 3.2 Image compression of Mordecai the snow dog, truncating the SVD at various ranks r. Original image resolution is 2000 × 1500 (Brunton & Kutz, 2019).

A final note of importance with SVD which will become important when discussing POD and DMD is the importance of orthogonality within the data-sets. Keep in mind that SVD attempts to find statistical characteristics in the data-set through element correlations. As such, for SVD to be as efficient as possible, the data-set should be organized so that structures should appear inline with both the rows and columns. This is not always possible as often SVD is needed to even identify correlations to begin with. However, whenever possible, it is best practice to make the data-set as orthogonal as possible. Take for example the case of simply taking SVD of an image of a square. If the square is positioned with the previously mentioned recommendations, the whole image can be compressed to a single rank. However, if the square is tilted by 10 degrees, the rank required is significantly different. Figure 3.3 illustrates the importance and meaning of orthogonality. While making the spatial correlations, SVD will only see a single repeating nonzero structure when looking from either the rows or columns. Every row or column which makes up the square has the same number of black and white spaces and as such is the only dominant structure of the image. On the other hand, with the image

tilted by 10 degrees, there are now many more ‘structures’ or columns/rows required to define the square. Again, while it is not always possible to perfectly align data-sets, when possible proper alignment of a data-set can led to a significant boost in performance of SVD.

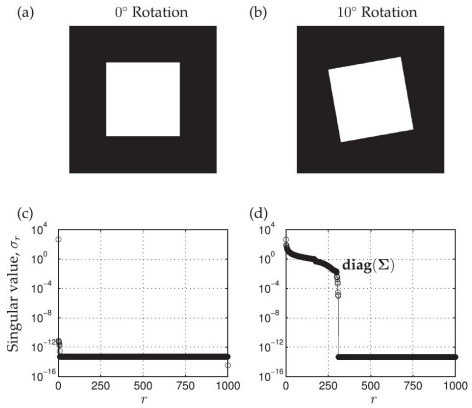

Figure 3.3 A data matrix consisting of ones with a square sub-block of zeros (a), and its SVD spectrum (c). If we rotate the image by 10 degrees, as in (b), the SVD spectrum becomes significantly more complex (d) (Brunton & Kutz, 2019).

3.3. Proper Orthogonal Decomposition

Now that a solid basis has been formed for the modal analysis a deeper look at the modal methods can be taken. The first of these methods to be incorporated into the fluid dynamics field was POD. The origins of POD can be traced back to 1901 through the work of Karl Pearson. In Pearson’s work he established a method for identifying correlations in data-sets called PCA. PCA eventually was altered and applied to various fields of science and engineering. In signal processing, PCA became the Karhunen-Loeve Transform (KLT), Hotelling transform in multivariate quality control, eigen value decomposition in linear algebra, and in mechanical engineering POD (Jolliffe, 2002). Even SVD, which is the basis for the POD method used in this study, is simply an evolution of PCA. Despite the importance of this algorithm to scientists and engineers today, for the first half of the 20th century PCA went largely unused because of the vast computational power required to analysis practical data-sets. It was not until the later half of the century that computational power began to become powerful enough to allow for PCA to be practical. Once PCA was clearly seen as a practical and efficient

method for classifying large data-sets many of the methods previously mentioned began development. POD was eventually fine tuned from PCA to assist fluid-dynamics engineers in identifying leading structures in physical systems of high degrees of freedom.

The premise of this method is to attempt, through spacial correlations, to find a low rank number of modes which can be use to reconstruct the original system. Since the algorithm is only looking at spatial correlations, the only weighting for the modes will be in terms of the total energy that they capture of the original system. Since the leading objective of POD is to identify perturbed structures of a scalar, the first step is to subtract out the averaged scalar term.

$$X_P = X - X_m \tag{13}$$

After obtaining this perturbation matrix the modes can quickly be obtained through first finding the correlation matrix and then computing the SVD. This correlation matrix can be found by simply multiplying the perpetuated matrix by the transpose of itself.

$$C = X_P X_P^T \tag{14}$$

To obtain the modes a simple SVD is taken of matrix C.

$$C = U\Sigma V^T \tag{15}$$

From here the modes are extracted from the U matrix. From the Σ matrix the singular values are extracted. The singular values in the Σ matrix are used to give insight into how much of the total energy of the system is represented by each mode.

$$\sigma_r = \frac{Diag(\Sigma_r)}{sum[Diag(\Sigma)]} * 100\% \tag{16}$$

The objective of POD is to retain the number of modes from the U matrix so that σ_r approaches a desired value. Typically, users will desire a σ_r convergence of around 90% with some desiring as high as 99%. The importance of these convergence criteria depends on the application and whether the user desires accuracy or compression of data.

Ultimately, in this investigation the desired convergence of the singular values was set to be 90%.

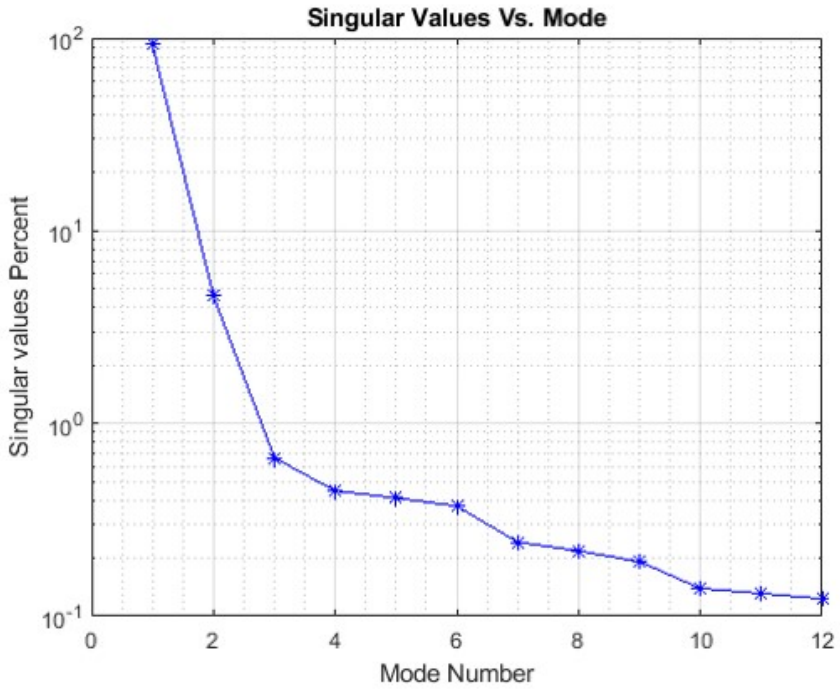

Figure 3.4 Singular Values Percentage

This leads to one of the greatest advantages of POD. The POD algorithm allows for a simple method for identifying not just the modes of a system, but more importantly provides a straightforward method for ranking the weighting of each mode on the original data-set. The ability to identify significant modes becomes of extreme importance as the spatial dimensions of the data-set become significantly large, say between 100,000 and 10,000,000. At data-set sizes of these magnitudes, it becomes impractical to try to visually identify structures in each mode and correlate their significant to the original system. Rather there needs to be a robust algorithm for confidently making these correlations. With POD there is such a method through simply using the Σ matrix.

Yet, despite the various advantages of the POD algorithm, there remains some disadvantages that are necessary to discuss. One of these disadvantages comes from the vast computational power required to complete a full SVD on a sufficiently large data-set. The two issues become time and memory. Simply computing SVD on a

50,000-by-50,000 matrix in MATLAB requires a total of 30 Gigabytes of RAM to compute.

Another potential disadvantage to POD is its inability to resolve heavily time dependent structures of the flow field. The POD algorithm is only looking to identify how element values change in space and ignores any variation in frequency of the structures. As such the ordering of snapshots in the snapshot matrix may not make a large impact on the modes or mode ordering. For structures in the flow field which appear in fixed growth rates this does not tend to lead to issues. However, when multiple structures begin to appear at varying frequencies, POD tends to operate very poorly.

Once these modes are obtained one can use the below relationship to project the selected subset of modes back onto the original perturbation matrix.

$$X_P = \Phi_r a_t \tag{17}$$

In Equation 17 the newly introduced term a_t is called the time coefficient. In essence, this term is simply a reconstructing term. In the event that it is desired to simply obtain a best fit of the modes back onto the original data-set, the Equation 18 can be used. For the modal analysis of the pitch up motion cases, this equation was used as the objective was to simply identify the capability of POD/DMD in resolving free-stream and surface pressure structures.

$$a_t = \Sigma_r V_r^T \tag{18}$$

After obtaining a_t, it becomes possible to construct a data-driven model for the system by recognizing first that a_t will be an array for each mode. The array found in Equation 18 will correspond to discrete points in time. At each of these points in time, both free-stream and body motion characteristic are defined. By taking an expansion of these terms, a function can be built relating these terms to a_t. This function now provides a continuous representation of the coefficients a_t. This continuous function can be used to build an aerodynamic model for a store at extremely low computational cost.

$$a_t = F(\alpha, q, U_\infty, \rho_\infty, T_\infty ...) \tag{19}$$

A interesting characteristic of a_t is the ability to identify a better understanding of energy content of each mode. The energy content of these modes can be defined as below (Lumley, 1981).

$$KE =< a_t >< a_t > \tag{20}$$

In Equation 20, KE is the total kinetic energy contribution of each mode at each time step. The rank of KE is the total number of time steps present in the data-set. By taking the FFT of this data-set, a spectrum for each of retained modes can be defined.

3.4. Dynamic Mode Decomposition

The other modal method used in this study was DMD. This method was developed by Schmid in the mid-2000s as a build off of POD (Schmid & Sesterhenn, 2008). As mentioned previously, POD undertakes no consideration of time dependency of structures in data-sets as it is based entirely on SVD. Thus, the use of only spatial dimensions has lead to a significant limitation in the application of POD to many fluid dynamics problems. This limitation is what leads to the direct desire to develop an alternative algorithm capable of resolving these temporal structures while still maintaining the robustness of POD. Such an algorithm was eventually developed through DMD which follows a similar path to that of the SVD based POD except that there is the additional consideration for temporal frequencies through a Fast Fourier Transformation (FFT). Since its inception, DMD has become an extremely popular tool for both its robustness and flexibility in the fields of control theory, multi-resolution techniques, and compressed sensing.

While many formulations of the DMD algorithm have been proposed since its inception, in this study the *exact* DMD framework will be presented. This DMD algorithm starts by first splitting the snapshot matrix into two matrices: one going from the first snapshot to the second to last and the other going from the second snapshot to the last.

$$u_x = [u(t_1), u(t_2), ...u(t_{n-1})] \tag{21}$$

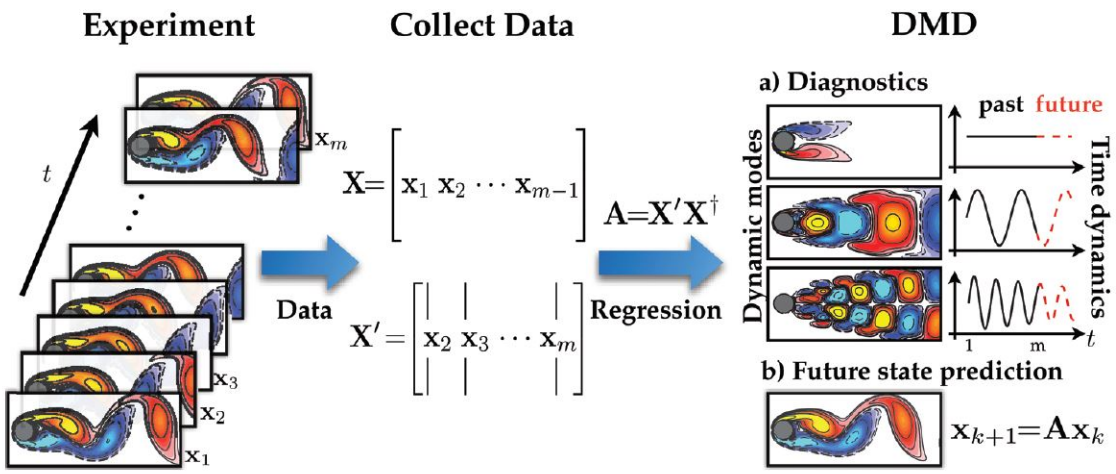

Figure 3.5 Overview of DMD illustrated by a cylinder (Brunton & Kutz, 2019).

$$u_y = [u(t_2), u(t_2), ...u(t_n)] \tag{22}$$

The below equation is then used to relate each snapshot to the snapshot one time step forward.

$$u_y = Au_x \tag{23}$$

From here, the eigenvalues λ and eigenvectors ω of the A matrix are found. λ become important later in the DMD algorithm when trying to correlate each mode back to the original data-set. ω is used in Equation 26 to include a weighting of frequency into the mode identification.

$$[\omega, \lambda] = eig(A) \tag{24}$$

Next, a SVD expansion of u_x is taken. It is through this equation that the spatial correlations are derived in the DMD algorithm.

$$SVD(u_x) = U\Sigma V^T \tag{25}$$

The final step is to combine Equations 23, 24, and 25 to obtain Equation 26.

$$\Phi = u_y V^T \omega / \Sigma \tag{26}$$

To summarize, time dependent correlations between each time step are first identified. Then an expansion of the u_x snapshot matrix using SVD is taken after which

the A matrix is expanded through an eigenvalue decomposition. This all arrives at Equation 26 for the DMD mode matrix. While this method includes more computation than POD, the major advantage is that now the user is given a set of modes which can potentially resolve high frequency structures in the flow field.

The biggest disadvantage of using DMD is that there is no longer a Σ matrix to provide the singular values which efficiently produces a ranking for how well each mode represents the original system. So now there is the non-trivial task of identifying which modes out of many of thousands, if not millions, best represent the system. The methods for efficiently identifying DMD modes are numerous, each having varying degrees of fidelity. However, this study will use the one which is most widely used. This method is often called the 'Unit Circle' approach. In this approach it is recognized that the eigenvalues of the A matrix will consist of both imaginary and real components.

$$\lambda = \lambda_r + i\lambda_i \tag{27}$$

The real components of lambda are taken to represent the growth/decay rates of the modes while the imaginary components represent the frequency of oscillation. If these eigenvalues are plotted in the complex plane, then a good visual is given to understand how well each mode represents the original system. Typically, the closer the eigenvalue aligns with the unit circle, the better the corresponding mode represents the system. However, just having the modes align with the unit circle does not guarantee the mode will represent the system well. Truly identifying the proper modes takes much time and effort. How much of a limiting factor this challenge becomes varies depending on its application.

For academic work, this tends not to be such a great issue. In academic, work the users of this method tend to work on their own schedule and thus have more time to look at multiple sets of modes. Yet in many industry applications, the DMD method can potentially be a tricky method to implement. Take, for instance, the potential application of this study. The eventual end goal of this study would be to develop a system which

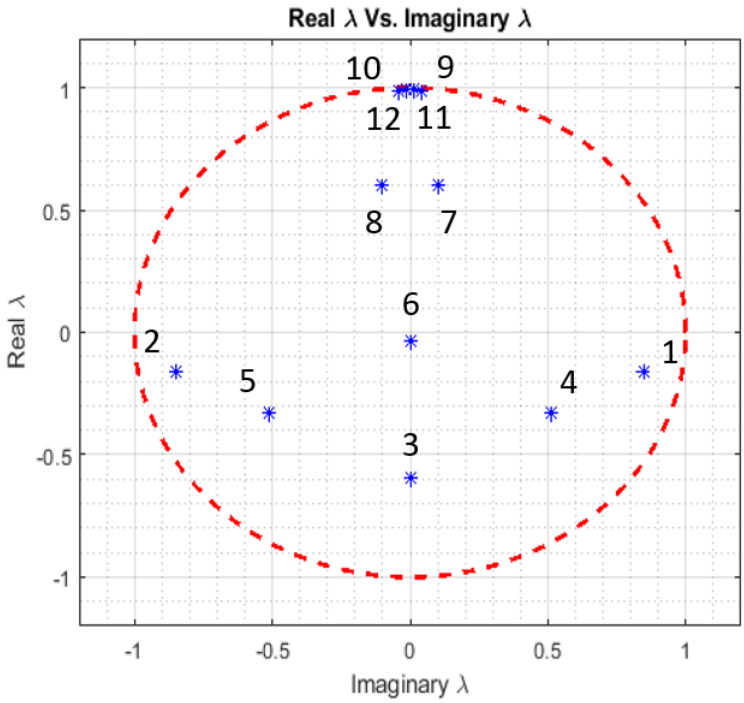

Figure 3.6 DMD eigenvalues plotted on the complex plane

could process store separation simulation data and export a robust mode-based ROM. In order to be competitive with current methods of analyzing store separation, this ROM must not only be more accurate than current models but must also be significantly faster to construct. Given that a 6-DOF model will always lack accuracy compared to a flight test, companies may feel that unless this new method of constructing a ROM is significantly faster, there may not be a point in overhauling their current techniques in the store separation analysis. In considering this, ability to identify modes quickly will be of major significance in this study.

In addition to mode identification there are many more additional challenges associated with DMD which can limit its application. To start with, DMD struggles to reconstruct traveling waves. This largely comes from the separation of variables between the time and spatial correlations. This separation of variables is a method which has proven to not capture traveling waves particularly well.

4. Overview of Experiment

As in any computational based study, validation of results are key to ensuring the findings of the study maintain a firm grounding in reality. However, being that this study is centered around store separation, obtaining well documented peer-reviewed experimental results is a significant challenge. As such, this study was not able to obtain detailed validation results for the transonic speeds being simulated. Rather, the study was required to validate its numerical models based of a series of subsonic experimental results (Wetzel, 1998). While these results were taken at subsonic speeds, the results do include extremely detailed documentation of not only experimental setup but also surface pressure data across various segments of the store. In this section, the experimental setup, flight conditions, and results will be summarized.

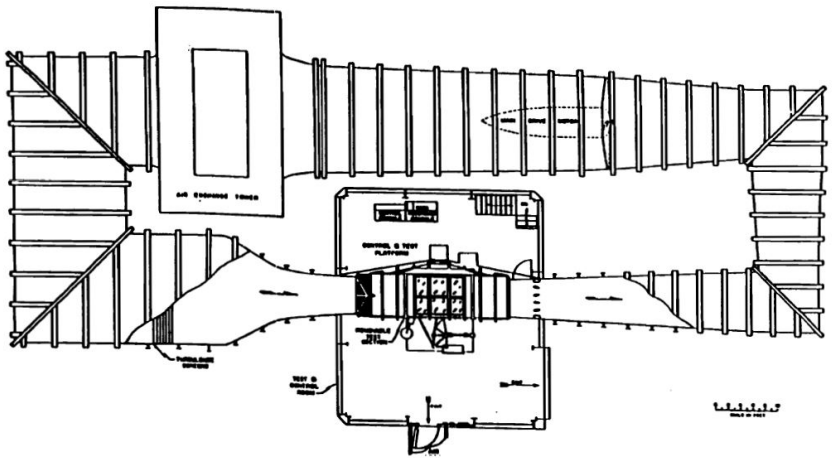

Figure 4.1 Virginia Tech Stability and Control Wind Tunnel (Wetzel, 1998).

The experiments completed by Wetzel were completed in the Virginia Tech Stability and Control Wind Tunnel in 1996 (Figure 4.1). The experiment was completed on a 1.372 meter long 6:1 prolate spheriod at a constant velocity of 45.7 m/s and a Reynolds number of $4.2 * 10^6$. The rear 10% of the store was removed to allow for the attachment of a sting to the store. This sting was then attached to a system which allowed for pitching, plunging, and rolling of the store (Figure 4.2).

For the transient validation between the numerical model and experiment, only one of the actuator arms was allowed to move. This motion results in the pitching up of the

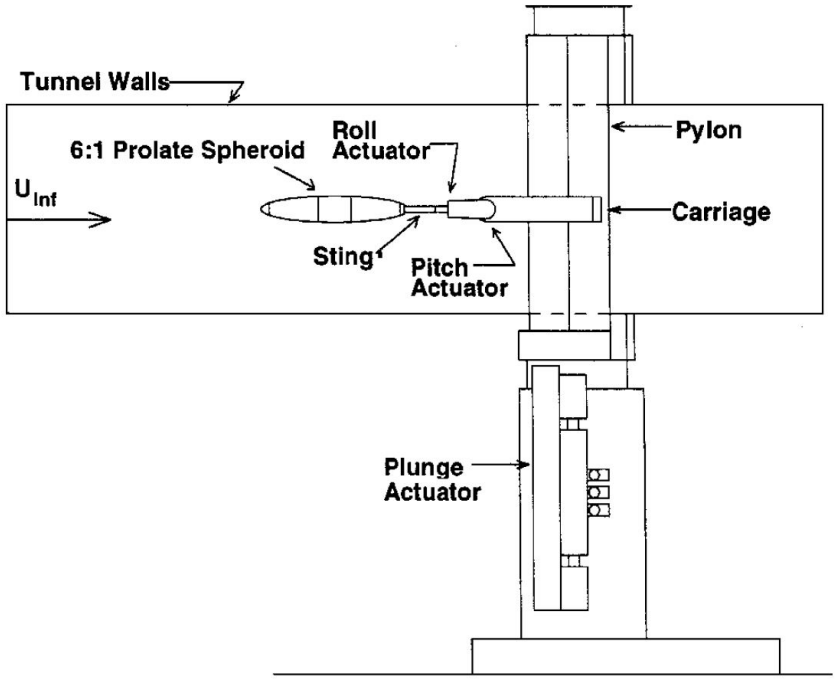

Figure 4.2 Experimental setup of store in wind tunnel (Wetzel, 1998).

store in a range of 0 to 30 degrees from the horizontal center line of the wind tunnel. The rate of pitch for this motion was 90 deg/s (Figure 4.3).

For the time averaged validation, only a single pitch angle was chosen. This angle was at 20 degrees. For this time averaged comparison, the results found in Figure 4.4 were used to validate surface pressures for the numerical model. Figure 4.5 was used as a comparison to ensure the proper vortex structures were being obtained.

For the transient model validation, the surface pressure coefficient results in Figures 4.6-4.8 were used. These results summarize the transient solutions as found by Wetzel for a 6:1 prolate spheriod and are compared directly to the steady state solution for each angle of attack. Here, the unsteadiness of the flow field can be observed as the instantaneous measurements are taken.

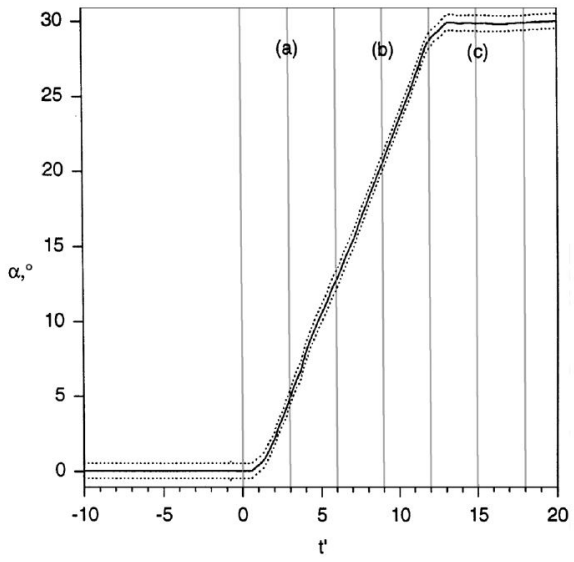

Figure 4.3 Pitch-up maneuver pitch angle position feedback verse time. Total motion happening over the course of 1/3 seconds (Wetzel, 1998).

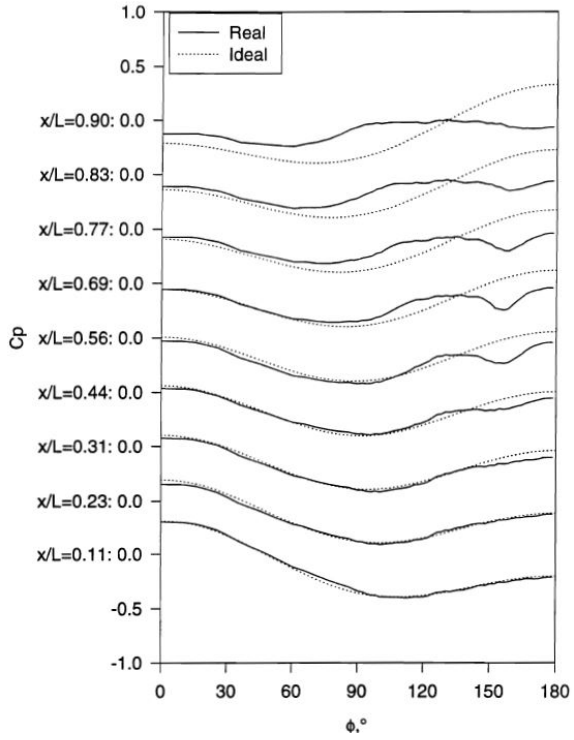

Figure 4.4 Time averaged coefficient of pressure verse angle across store for all x/L at a pitch of 20 degrees. 'Real' refers to the measured data while 'ideal' refers to potential flow solution (Wetzel, 1998).

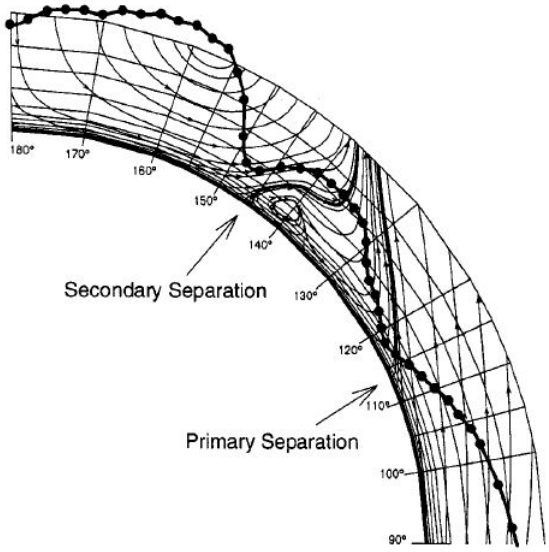

Figure 4.5 Primary and secondary separation locations along with free-stream structures (Wetzel, 1998).

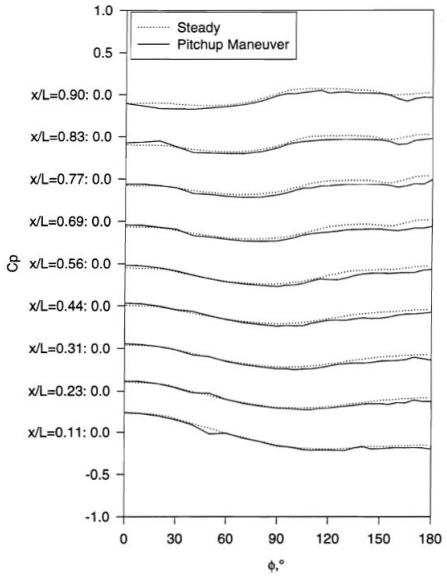

Figure 4.6 Transient coefficient of pressure verse angle across store for all x/L at a pitch of 15 degrees (Wetzel, 1998).

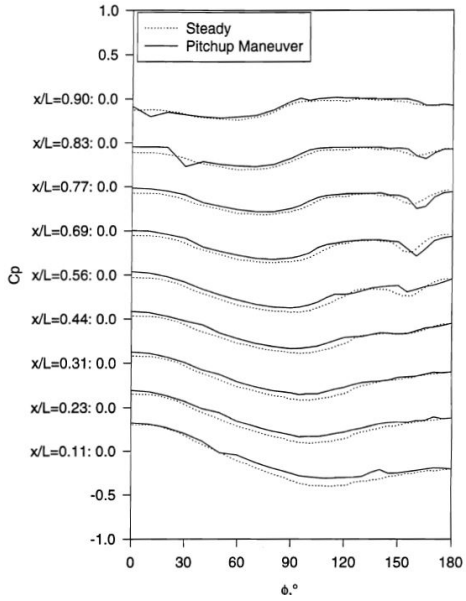

Figure 4.7 Transient coefficient of pressure verse angle across store for all x/L at a pitch of 20 degrees (Wetzel, 1998).

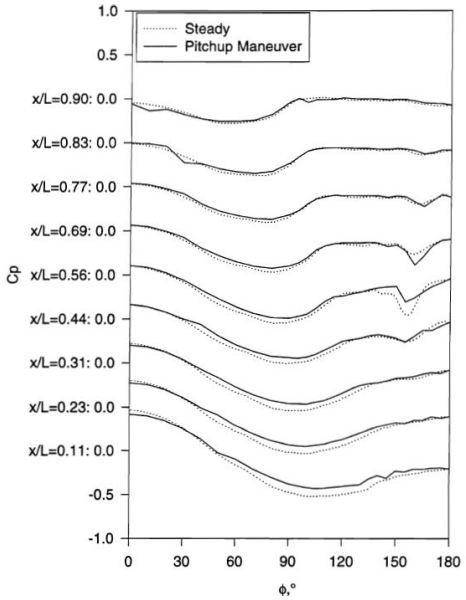

Figure 4.8 Transient coefficient of pressure verse angle across store for all x/L at a pitch of 25 degrees (Wetzel, 1998).

5. Numerical Modeling

The numerical modeling used in this study was based around the compressible flow variation of the Navier-Stokes (N-S) equations. These equations governing the conservation of mass, three dimensional momentum, and energy for the model are outlined in Einstein notations below in Equations 28, 29, and 30 (White & Corfield, 2006).

$$\frac{\partial \rho}{\partial t} + \frac{\partial \rho u_i}{\partial x_i} = 0 \tag{28}$$

$$\left(\frac{\partial \rho u_i}{\partial t} + \frac{\partial \rho u_j u_i}{\partial x_j}\right) = -\frac{\partial P}{\partial x_i} + \frac{\partial \tau_{ij}}{\partial x_j} + \rho f_i \tag{29}$$

$$\left(\frac{\partial \rho E}{\partial t} + \frac{\partial \rho u_j E}{\partial x_j}\right) = -\frac{\partial P u_j}{\partial x_j} + \frac{\partial u_i \tau_{ji}}{\partial x_j} + \frac{\partial q_j}{\partial x_j} \tag{30}$$

In these equations f_i serves to represent any source term adding or subtracting momentum from the system, *E* serves as the total energy in the system, q_i is the conduction of heat through the system, and τ_{ij} is the viscous stresses. The specific equations for these variables are outlined below.

$$E = e + \frac{1}{2} u_i u_i \tag{31}$$

$$q_j = -k \frac{\partial T}{\partial x_j} \tag{32}$$

$$\tau_{ij} = \mu \left(\frac{\partial u_i}{\partial x_j} + \frac{\partial u_j}{\partial x_i}\right) - \frac{2}{3} \mu \frac{\partial u_k}{x_k} \delta_{ij} \tag{33}$$

Here μ is viscosity, e is internal energy, and k is conductivity. The final stage of these equations is to relate pressure to density and identify how to calculate laminar viscosity. For relating pressure to density this is completed through the usage of the ideal gas law. This provides an algebraic way to correlation not only between pressure and density but also with temperature. Once these variables are identified the laminar viscosity can be defined through use of Sutherland's Law.

$$P = \rho R T \tag{34}$$

$$\mu = \mu_{ref} \left(\frac{T}{T_{ref}}\right)^{3/2} \frac{T_{ref} + S}{T + S} \tag{35}$$

5.1. Turbulence Modeling

One of the most daunting challenges of the past several decades has been to develop computational methods for modeling turbulent flows. Part of the difficulty around developing such models derived from the fact that turbulence is by nature extremely chaotic, making it difficult to model in the traditional N-S equations. By reviewing Equations 28, 29, and 30, it is quickly observed that there are now stochastic terms to model turbulence in the traditional N-S equations. To model turbulence, a manipulation of these equations must be undertaken called Reynolds averaging which transforms the N-S equations into the Reynolds Averaged Navier Stokes equations (RANS).

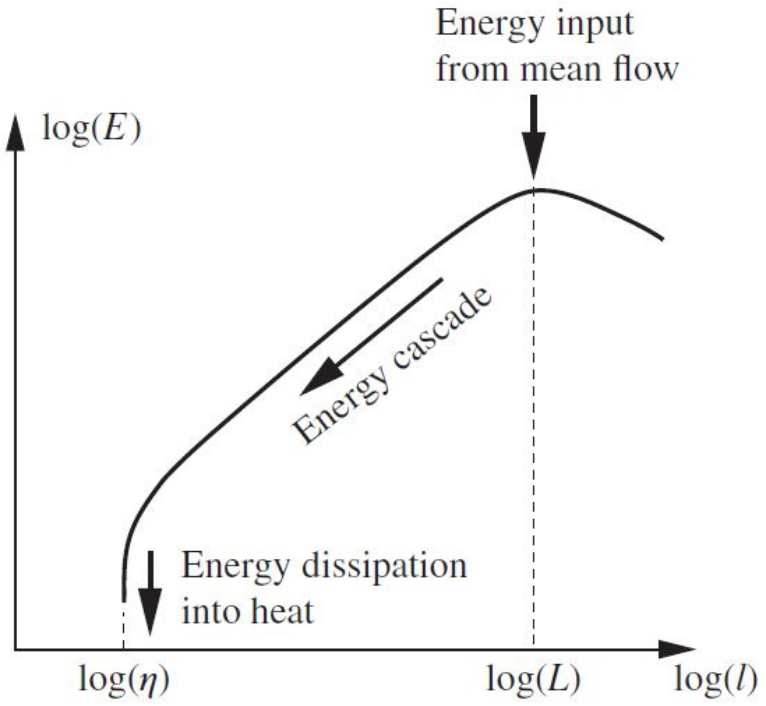

Figure 5.1 Schematic representation of the distribution of energy of velocity fluctuations over the length scales in a turbulent flow (Pope, 2001).

A common question may arise as to why the original form of the N-S equations cannot be used. To answer this question, a concept called the energy cascade must first be discussed. The energy cascade is an idea that turbulence first begins as large eddies in the flow field. While there is no exact agreed upon definition for what these eddies are, they can generally be understood as singular large coherent structures of the flow

field. These large eddies contain the largest turbulent energy of the flow field. These large eddies then devolve and breakdown into smaller eddies which then break down to even smaller eddies, with each eddy containing less energy than the last. Eventually these eddies break down to such a small size that, rather than breaking down any further, they simply dissipate into heat. This cascade is represented in Figure 5.1. From here a good understanding is obtained as to over why it is necessary to model turbulence. In Figure 5.1, η represents the Kolmogorov scale, the scale at which an eddy will dissipate into heat rather than cascade further down. In order to properly resolve turbulence in a computational model using a grid, the Δx_i spacing of nodes must be of the same size as η. The issue with this is quickly realized by starting with Equation 36.

$$\frac{L}{\eta} = Re^{3/4} \tag{36}$$

In Equation 36, assume L to be the one dimensional length of the computational domain. This means that in just one dimension, the total number of nodes needed in the computational domain is $Re^{3/4}$. Note that this is simply for a singular dimension of the domain; to resolve all three dimensions, this number becomes much larger as outlined in Equation 37.

$$\frac{L_x}{\eta} * \frac{L_y}{\eta} * \frac{L_z}{\eta} = Re^{9/4} \tag{37}$$

This begins to illustrate the extreme difficulty is modeling even the most simple of aerodynamic problems using the full N-S equations. It also highlights the need for use of RANS modeling the for many fluid dynamic problems.

5.2. RANS Models

Rather than attempting to resolve all the scales of turbulence in the flow field, RANS modeling attempts to solve only the largest eddies of the flow field. From here, the remainder of the energy cascade is modeled with stochastic terms. It is because of this that, through RANS modeling, the number of nodes in the computational grid can be significantly reduced while still maintaining a large amount of the energy in the fluid system. The process of developing the RANS equations begins with first introducing a

new form of the u_i velocity, Equation 38.

$$\Phi_i = \bar{\Phi}_i + \Phi_i' \tag{38}$$

Equation 38 simply states that for every state variable Φ_i there exists an average term $\bar{\Phi}_i$ and a perturbation term Φ_i'. Equation 38 is then substituted into Equations 28, 29, and 30. From here, a Favre-averaging is completed on the velocity and energy equations, resulting in a new variable Θ which is a function of ρ and u.

$$\Theta_i = \widetilde{\Theta}_i + \Theta_i' \tag{39}$$

$$\widetilde{\Theta}_i = \frac{\overline{\rho\Theta}}{\bar{\rho}} \tag{40}$$

The resulting RANS formulas are presented in Equations 41, 42, and 43.

$$\frac{\partial \bar{\rho}}{\partial t} + \frac{\partial \bar{\rho}\widetilde{u}_i}{\partial x_i} = 0 \tag{41}$$

$$\left(\frac{\partial \bar{\rho}\widetilde{u}_i}{\partial t} + \frac{\partial \bar{\rho}\widetilde{u}_j\widetilde{u}_i}{\partial x_j}\right) = -\frac{\partial \bar{P}}{\partial x_i} + \frac{\partial}{\partial x_j}\left(\overline{\tau_{ij}} - \overline{\rho u_i' u_j'}\right) \tag{42}$$

$$\left(\frac{\partial \bar{\rho}\widetilde{E}}{\partial t} + \frac{\partial \bar{\rho}\widetilde{u}_j\widetilde{E}}{\partial x_j}\right) = -\frac{\partial \bar{P}\widetilde{u}_j}{\partial x_j} + \frac{\partial \overline{u_i\tau_{ji}}}{\partial x_j} - \frac{\partial \bar{q}_j}{\partial x_j} - \frac{\partial \overline{u_j'' P}}{\partial x_j} - \frac{\partial \overline{\rho u_j'' E''}}{\partial x_j} \tag{43}$$

From this expansion of the N-S equations, new terms appear which represent the stochastic variables for turbulence. While there have been numerous models proposed to solve for these stochastic variables, there will be two which are reviewed and used in this study, the Spalart-Allmaras and the K-W SST turbulence models. Note, there are far more turbulence models which exist outside of the Spalart-Allmaras and K-W SST model. However, given the time limitations imposed on this study, these alternative models were not investigated and thus will not be reviewed.

5.2.1. Spalart-Allmaras

The first of these two models to be developed was the Spalart-Allmaras single equation turbulence model (Spalart & Allmaras, 1992). The model is known to be both extremely robust and computationally efficient. Much of this derives from the fact that there is simply a single equation used to model the turbulence in this model. In the Spalart-Allmaras model, the turbulent eddy viscosity is calculated through the below

transport equation.

$$\nu_t = \widetilde{\nu} f_{v1} \tag{44}$$

$$f_{v1} = \frac{X^3}{X^3 + C_{v1}^3} \tag{45}$$

$$X = \frac{\widetilde{\nu}}{\nu} \tag{46}$$

The Reynolds Stresses are then calculated.

$$-\rho\overline{u_i' u_j'} = \rho\widetilde{\nu} f_{v_1} \left(\frac{\partial \widetilde{u}_i}{\partial x_j} + \frac{\partial \widetilde{u}_j}{\partial x_i} \right) \tag{47}$$

Finally the transport equation is set up for $\widetilde{\nu}$ to solve for the eddy viscosity.

$$\frac{\partial \widetilde{\nu}}{\partial t} + u_j \frac{\partial \widetilde{\nu}}{\partial x_j} = C_{b1} \left[1 - f_{t2}\right] \widetilde{S} \widetilde{\nu} + \frac{1}{\sigma} \left[\nabla \bullet \left[\left(\nu + \widetilde{\nu}\right) \nabla \widetilde{\nu} \right] + C_{b2} |\nabla \widetilde{\nu}|^2 \right] \tag{48}$$

Each variable in Equation 48 is defined below.

$$\widetilde{S} = S + \frac{\widetilde{\nu}}{k^2 d^2} f_{v2} \tag{49}$$

$$f_{v2} = 1 - \frac{X}{1 + X f_{v1}} \tag{50}$$

$$f_w = g \left[\frac{1 + C_{w3}^6}{g^6 + C_{w3}^6} \right]^{1/6} \tag{51}$$

$$g = r + C_{w2} \left(r^6 - r \right) \tag{52}$$

$$r = \frac{\widetilde{\nu}}{\widetilde{S} k^2 d^2} \tag{53}$$

$$f_{t1} = C_{t1} g_t exp \left(-C_{t2} \frac{w_t^2}{\Delta U^2} \left[d^2 + g_t^2 d_t^2 \right] \right) \tag{54}$$

$$f_{t2} = C_{t3} exp \left(-C_4 X^2 \right) \tag{55}$$

$$S = \sqrt{2\Omega_{ij}\Omega_{ij}} \tag{56}$$

$$\Omega_{ij} = \frac{1}{2} \left(\frac{\partial u_i}{\partial x_j} - \frac{\partial u_j}{\partial x_i} \right) \tag{57}$$

The constants in this model are defined in Table 5.1.

5.2.2. K-W SST

The K-W SST model is a two equation turbulence model created by Menter (1998).

Table 5.1

Constants used in the Spalart-Allmaras turbulent model

Constants	**Values**
σ	2/3
C_{b1}	0.1355
C_{b2}	0.622
k	0.41
C_{w1}	$C_{b1}/k^2 + (1 + C_{b2})/\sigma$
C_{w2}	0.3
C_{w3}	2
C_{v1}	7.1
C_{t1}	1
C_{t2}	2
C_{t3}	1.1
C_{t4}	2

The K-W SST model incorporates two equations to solve for the eddy viscosity as opposed to the single equation Spalart-Allmaras model. These two equations are based around solving for the turbulent kinetic energy and the specific dissipation rate. The K-W SST model, while more computationally expensive than the Spalart-Allmaras model, is known to preform extremely well in adverse pressure gradients and in separating flow. This makes the model of particular interest in this study where identifying flow structures with the store at high angles of attack is of particular interest. In this model, the eddy viscosity is found by the below relationship.

$$\nu_T = \frac{a_1 k}{max\left(a_1\omega, SF_2\right)} \tag{58}$$

$$\frac{\partial k}{\partial t} + U_j\frac{\partial k}{\partial x_j} = P_k - \beta k\omega + \frac{\partial}{\partial x_j}\left[\left(\nu + \sigma_k\nu_T\right)\frac{\partial k}{\partial x_j}\right] \tag{59}$$

$$\frac{\partial \omega}{\partial t} + U_j\frac{\partial \omega}{\partial x_j} = \alpha S^2 - \beta\omega^2 + \frac{\partial}{\partial x_j}\left[\left(\nu + \sigma_k\nu_T\right)\frac{\partial \omega}{\partial x_j}\right] + 2\left(1 - F_1\right)\sigma_{\omega 2}\frac{1}{\omega}\frac{\partial k}{\partial x_i}\frac{\partial \omega}{\partial x_i} \tag{60}$$

$$F_2 = tanh\left[\left[max\left(\frac{2\sqrt{k}}{\beta\omega y}, \frac{500\nu}{y^2\omega}\right)\right]^2\right] \tag{61}$$

$$P_k = min\left(\tau_{ij}\frac{\partial U_i}{\partial x_j}, 10\beta k\omega\right) \tag{62}$$

$$F_1 = tanh\left[\left[min\left[max\left(\frac{2\sqrt{k}}{\beta\omega y}, \frac{500\nu}{y^2\omega}\right), \frac{4\sigma_{\omega 2}k}{CD_{k\omega}y^2}\right]\right]^4\right] \tag{63}$$

$$CD_{k\omega} = max\left(2\rho\sigma_{\omega 2}\frac{1}{\omega}\frac{\partial k}{\partial x_i}\frac{\partial \omega}{\partial x_i}, 10^{-10}\right) \tag{64}$$

The constants in this model are defined Table 5.2.

Table 5.2

All constants used in the K-W SST turbulent model

Constants	**Values**
α_1	5/9
α_2	0.44
β_1	3/40
β_2	0.0828
β^*	9/100
σ_{k1}	0.85
σ_{k2}	1
$\sigma_{\omega 1}$	0.5
$\sigma_{\omega 2}$	0.856

5.3. ANSYS FLUENT

All simulations were completed using the CFD commercial solver FLUENT. FLUENT is a finite volume based CFD code currently owned and maintained by the computer software company Ansys Inc.. FLUENT allows for use of both structured and unstructured meshes to assist in solving for a wide range of fluid dynamic based problems. Some examples include, but are not limited too, steady-state/transient problems, in-compressible/compressible flow, thermal analysis, and structural-fluid coupling.

5.3.1. Finite Volume Method

To solve for the flow field, ANSYS uses a method called Finite Volume Method. While there are other schemes for CFD solvers, the finite volume method is by far the most commonly found method in commercial solvers. This is for two primary reasons: convenience of use with unstructured grids, and its property of global conservation

(Zikanov, 2019).

The finite volume method can be explained starting with the formal conservation equation (Equation 65):

$$\frac{d}{dt}\int_{\Omega}\Phi d\Omega = -\int_{S}\Phi V\cdot ndS + \int_{s}X\nabla\Phi\cdot ndS + \int_{\Omega}d\Omega \tag{65}$$

In Equation 65, $\frac{d}{dt}\int_{\Omega}\Phi d\Omega$ is the rate of change of Φ within Ω, $-\int_{S}\Phi V\cdot ndS$ is the convective flux and describes the convection of Φ by a velocity V, and $\int_{s}X\nabla\Phi\cdot ndS$ is then diffusive flux. Finally, $\int_{\Omega}d\Omega$ is a source term.

This integral now needs to be discretized to allow for numerical integration. The easiest way to do this is through a dot product between the cells volume $|\Omega|$ and the mean value of the integral determined through grid point values (Equation 66).

$$\int_{\Omega}\Phi d\Omega = \overline{\Phi}|\Omega| \tag{66}$$

This discretized integral can then be applied to a wide variety of 1-d to 3-d grids with both structured and unstructured cell types as illustrated by Figure 5.2.

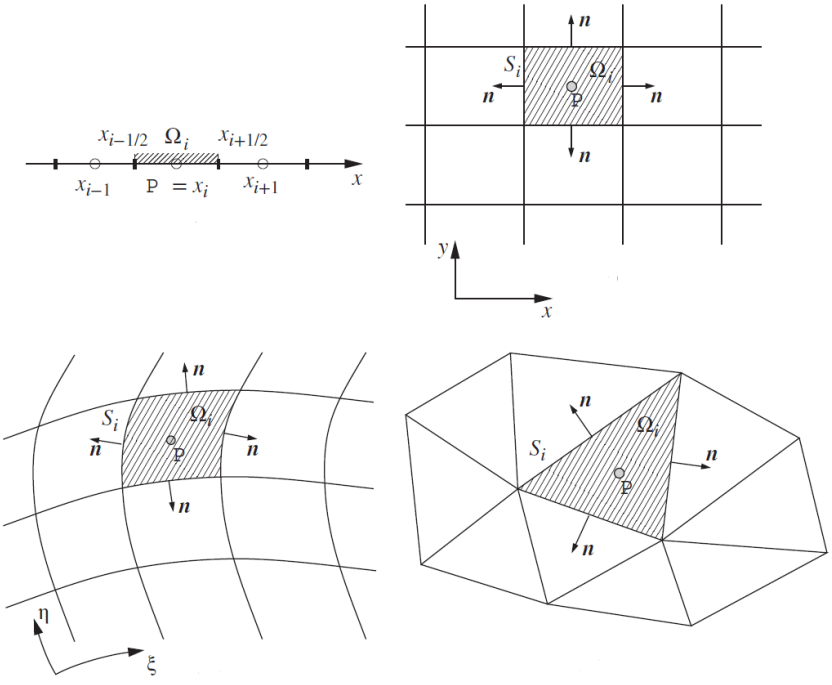

Figure 5.2 Examples of finite volume method applied to a wide array of cell types (Zikanov, 2019).

5.4. Mesh Generation

All meshes generated for this study were completed using the modeling software Pointwise. To maintain good orthogonality in the grid the meshes were constructed using structured cells. To start, a curve was drawn which represented one half of a 6:1 ellipse. This curve was lined with 300 axial nodes and revolved 360 degrees around the X-axis using 180 circumference nodes.

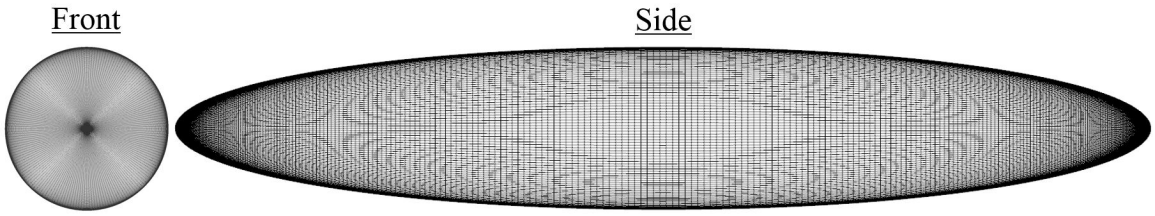

Figure 5.3 Surface mesh used for 6:1 prolate spheriod.

A mesh refinement study was completed to ensure a mesh independent solution was formed. In this mesh refinement the total number of circumference nodes was doubled to 360 nodes.

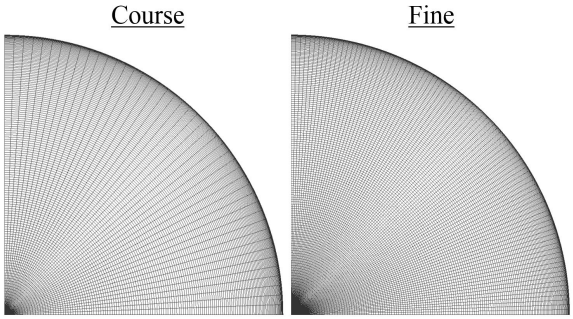

Figure 5.4 Forward quater view of both the coarse mesh, right, and the fine mesh, left.

5.4.1. Pitch Up Mesh

For the case of the pitch up motion the mesh was extruded 20 chord lengths away from the store.

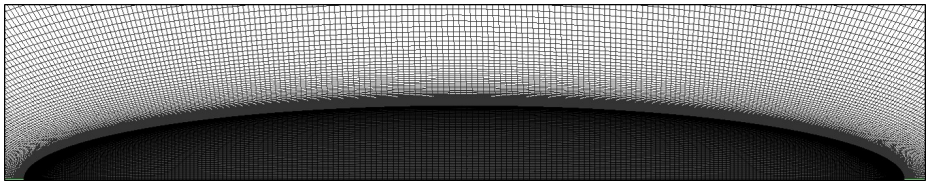

Figure 5.5 Near field extruded mesh for the pitch up motion case.

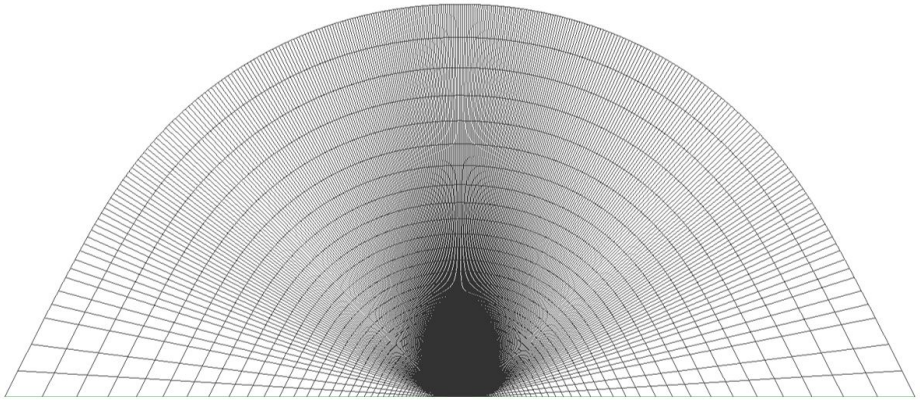

Figure 5.6 Far field extruded mesh for the pitch up motion case.

5.4.2. Overset Meshing

An important technique used to construct the mesh for the store separation cases in this study is called overset meshing. Overset meshing is a technique often used to help maintain grid quality for meshes with multiple independent bodies. Examples include fighter jets with complex store configurations, a full Space Shuttle model, detailed modeling for sports car, etc.. In all of these examples, the issue of conjoining well constructed meshes from each individual body becomes a non-trivial task. This issue is exacerbated when the independent dynamics of these bodies are being considered as well. In these cases, such as the case of store separation modeling, it becomes very difficult to maintain proper mesh refinement without the use of the technique of overset meshing.

Overset meshing begins with considering two independent grids. One is the major grid and one is the minor grid. These two grids are first overset on top of one another. A hole is then cut in the major grid to allow room for the minor grid. This cut allows for an overlap region in the mesh between the major and minor grids. As the simulation is being run, calculations are completed on the minor and major grids. Information is passed between the two grids through the overlap region of the grid through an interpolation.

Figure 5.7 provides a visual summary of the concept of overset meshing.

It should be noted that there is an alternative method for mesh control under dynamic modeling called Dynamic Meshing. In Dynamic Meshing the simulation first allows the boundary of interest to move/deform. In each time step in the solution, the full mesh is reconstructed. The previous solution is then interpolated on to the new grid before moving onto the next time step. The major advantage in this solution is that grid continuity is properly maintained. Meaning, traveling waves will not be deformed as they travel across the overlap region of two separate meshes.

However, Dynamic Meshing was not used for the simple fact that this method alters the spacial dimensions of the solution at each time step. This unfortunately leads to the method being not practical for the case POD/DMD which require a constant spacial dimension for the snapshot matrix.

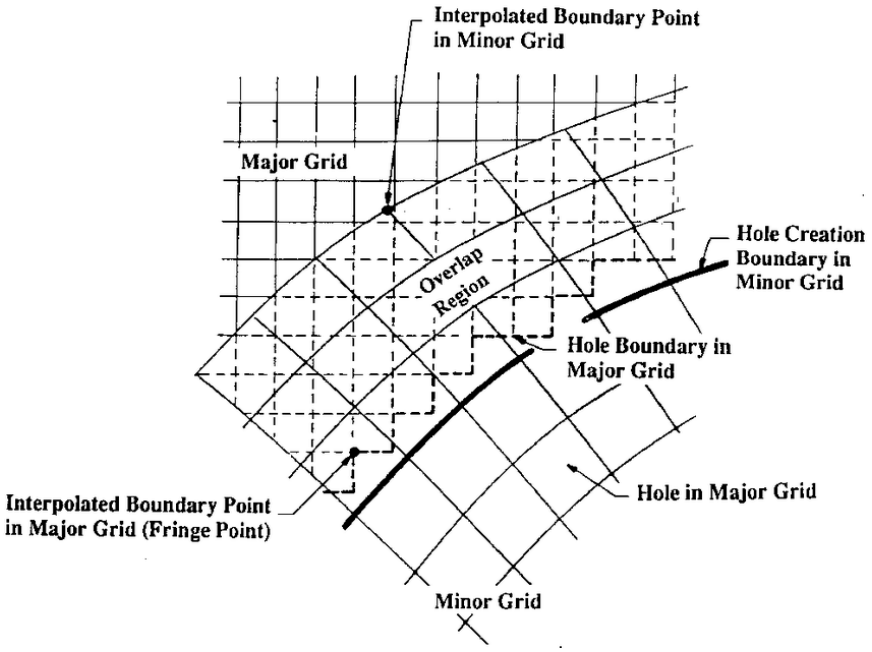

Figure 5.7 Graphic summarizing the premise of overset meshing (Ramakrishnan & Scheidegger, 2016).

5.4.3. Store Separation Mesh

For the store separation mesh, two independent meshes were first constructed and then stitched together using the overset meshing technique. For the background mesh, the study started with the coarse mesh which was used for the pitch up case. For the store

separation cases, there needed to be a higher resolution to the mesh in the field which the store would be traveling through. As such the only difference made between the store separation background mesh and pitch up mesh was that the field nodes were constricted closer to the wall (Figure 5.8).

To construct the stores mesh, the study first scaled the surface mesh for pod (Figure 5.3) down by a factor of 1/4. A mesh was then extruded from the surface of the store (Figure 5.9). The background and store meshes were then combined together through FLUENT's overset meshing tool set (Figure 5.10).

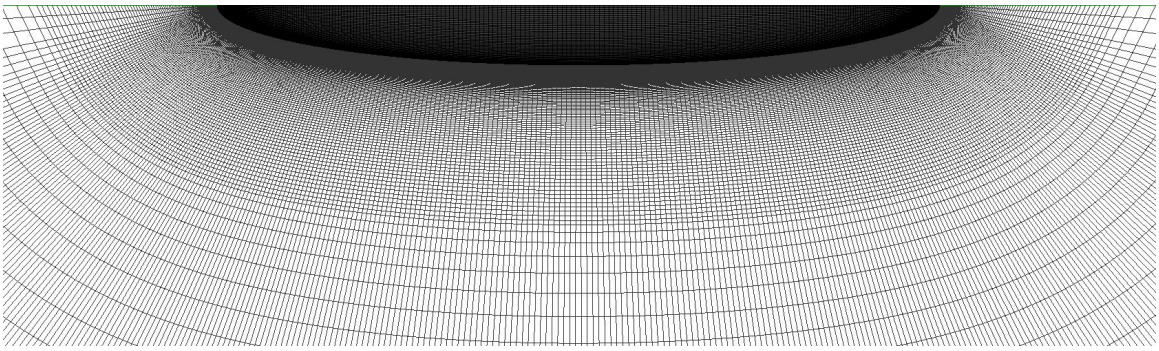

Figure 5.8 Near field extruded mesh for the store separation case.

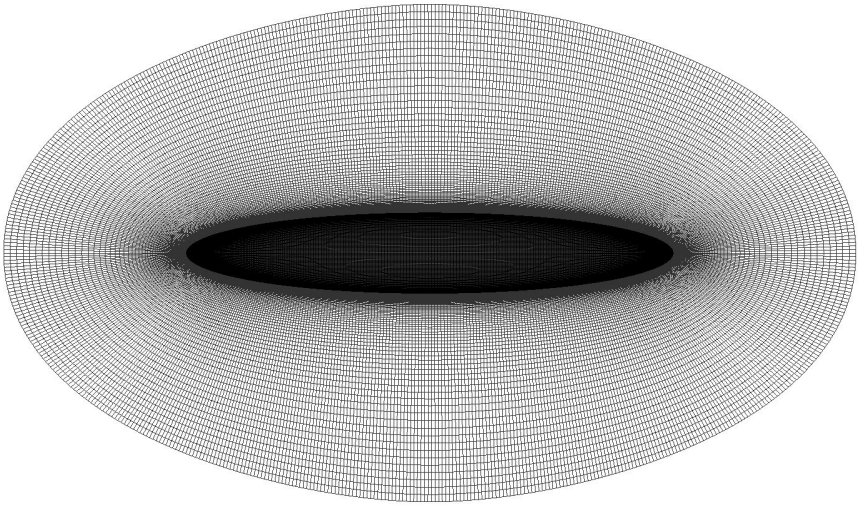

Figure 5.9 Near field extruded mesh for the store separation case.

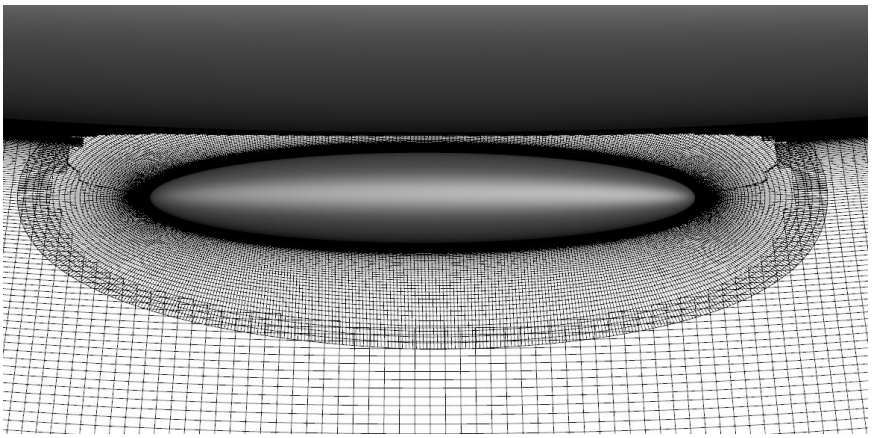

Figure 5.10 Near field extruded mesh for the store separation case.

5.5. 3-Degree of Freedom Modeling

As a final step for this study a 3-dof model was constructed using a limited number of modes as the aerodynamic model. The study chose to construct a 3-dof instead of a 6-dof model as the simulation results indicated there to be a symmetry in the surface pressures on the z-plane of the body. The body axis equations of motion used in this model are presented below.

$$\ddot{x} = \frac{F_x}{m} \tag{67}$$

$$\ddot{y} = \frac{F_y}{m} - g \tag{68}$$

$$\ddot{\Theta} = \frac{M_z}{I_{yy}} \tag{69}$$

The acceleration equations are then converted first into velocities and then into positions through the below basic equations.

$$\dot{x}_{k+1} = \dot{x}_k + \Delta t \ddot{x}_k \tag{70}$$

$$x_{k+1} = x_k + \Delta t \dot{x}_k \tag{71}$$

5.5.1. Aerodynamic Model

In this section the aerodynamic model used to obtain the forces and moments in this 3-dof model will be reviewed. This model begins with first selecting a limited number of

surface pressure modes obtained through the modal analysis r.

$$\Phi_r \tag{72}$$

These modes are then projected back onto the original data-set through Equation 73.

$$P = \Phi_r a_t \tag{73}$$

For each r series of a_t a linear interpolated function is created which relates the time coefficients a_t to the angle of attack α of the store.

$$F_r(\alpha) = a_{t_r} \tag{74}$$

At each timestep in the 3-dof model the surface pressures are updated through $F_r(\alpha)$. The surface pressures are then converted to forces and moments through the below equations.

$$F_x = PA_{cell}\hat{i} \tag{75}$$

$$F_y = PA_{cell}\hat{j} \tag{76}$$

$$M_z = PA_{cell}\hat{j}x - PA_{cell}\hat{i}y \tag{77}$$

In these equations P is an array of cell centered pressures, A_{cell} is an array consisting of cell areas, x/y are x and y cell centered positions respectively, and $\hat{i}/\hat{j}$ are x and y direction unit vector components respectively.

6. Simulation

In this section of the report, all simulation results will be presented and discussed. The pitch up case will be reviewed first. These cases will be broken down into steady-state and transient results. The single store separation case at Mach 0.8 will be reviewed next.

6.1. Pitch Up

Before looking at the pitch up results, the method for extracting the surface pressures and how they are presented is reviewed. This was done by taking slices at four separate chord lengths along the length of the store. These positions were 90%, 83%, 77%, and 69% chord length. From here, pressure measurements were taken from 0 degrees (the bottom of the store) to 180 degrees (to top of the store). These pressures were then normalized to find coefficients of pressure before being compared to the experiment. This process is outlined for the reader in Figures 6.1 and 6.2.

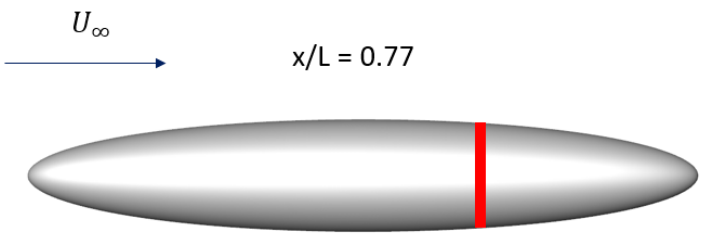

Figure 6.1 Example of slice being taken at a normalized cord length of 0.77. Side view

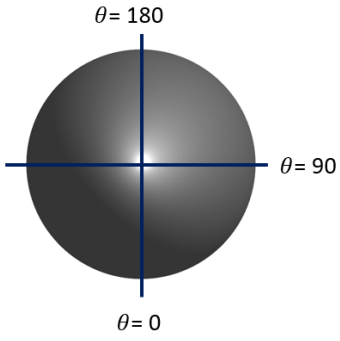

Figure 6.2 Example of slice being taken at a normalized cord length of 0.77. Head on view

6.1.1. Steady-State

To start, the steady-state solutions will be summarized and compared to the

experimental results. In total, 8 steady-state cases were run at an α of 20 degrees and a Reynolds number of $4.2 * 10^6$. The model selection of each case is summarized in the table below.

Table 6.1

Summary of all eight cases run in the steady-state for initial validation.

Turbulence Model	**Curvature Correction**	**Mesh Refinement**
K-W SST	Off	Coarse
K-W SST	Off	Fine
K-W SST	On	Coarse
K-W SST	On	Fine
SA	Off	Coarse
SA	Off	Fine
SA	On	Coarse
SA	On	Fine

By using the coarse mesh (Figure 7.6) the effect of using the four turbulence models were identified. When looking at the surface pressure results, an initial flat lining of the graph between 100-120 degrees is observed. This is a result of the primary separation, and the results show that in all models the primary separation location was accurately identified. The following dip in pressure that is observed is a result of the secondary separation location (reference Figure 4.5 for experimental secondary separation). At the 77% chord line, neither the S-A nor K-W SST models were able to accurately identify the strength of separation or phase. However, with the curvature corrections turned on both phase and magnitude of separation were nicely predicted. These results should come as no surprise; the curvature corrections implemented in the turbulence models are directly implemented to help model curvature of streamlines in the free-stream flow. Without these corrections these turbulence models will often struggle to predict heavily separated flow structures with large curvatures in streamlines. An additional important conclusion from these results is that there appears to be an independent solution to using a two equation turbulence model over a single equation model.

When observing the results from the mesh refinement it is observed in Figures

6.4 and 6.5 that the effect of doubling the circumferential nodes in the model does not provide any additional accuracy. This is to say that all structures that form in the Φ direction are mesh independent.

It should be noted that one additional case was run in an attempt to better model the secondary separation location on the store. Note that, at the x\L = 0.69 position, the phase of the secondary separation is delayed in the model. It is believed that this is the result of the simulation not properly modeling the boundary layer transition. This has historically been an issue for CFD codes and would explain why the magnitude of the separation is modeled correctly while the phase is not. In an attempt to better model this transition, an additional case was run with the coarse K-W SST curvature correction model with an additional transition model native to FLUENT turned on. The results shown in Figure 6.6 indicate that the addition of transition modeling considerations complicated the solution rather than providing a more accurate solution.

Now that it has been shown that using the S-A curvature correction model with the coarse mesh provides a good comparison with experimental results, it just needs to be shown that the free-stream structures do in fact appear in the model. These structures are shown in Figure 6.7. In this Figure, iso-surfaces of Q-criterion are shown passing through slices of vorticity magnitude. Surface flow patterns are represented through oil streaks. Here, the iso-surfaces of Q-criterion pass directly through the peaks of vorticity magnitude. This gives backing to the claim that the structures shown in Figure 6.7 are infact the desired primary and secondary vortex structures.

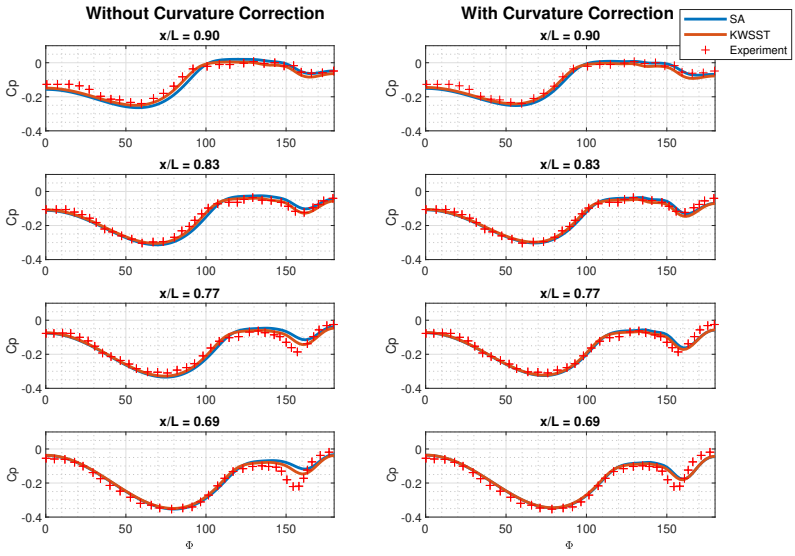

Figure 6.3 Surface pressure for coarse and fine mesh simulations compared to experiment. $\alpha = 20deg$ $Re = 4.2 * 10^6$

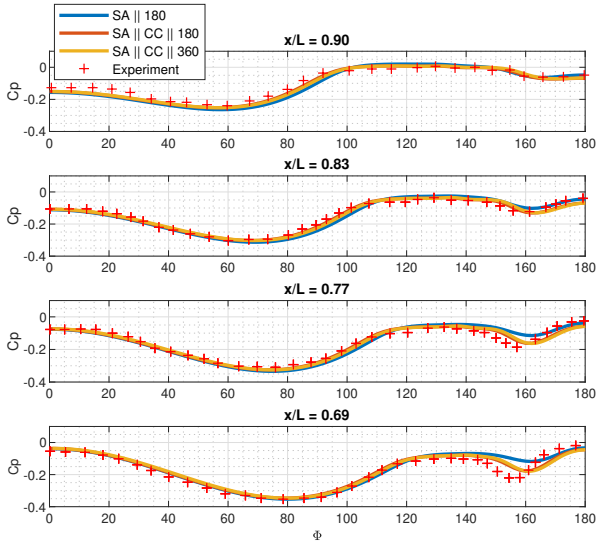

Figure 6.4 Surface pressure for all S-A simulations compared to experiment. $\alpha = 20deg$ $Re = 4.2 * 10^6$

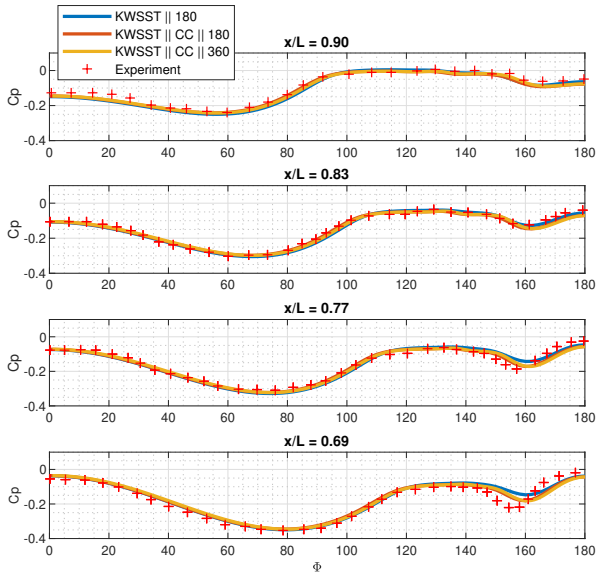

Figure 6.5 Surface pressure for all K-W SST simulations compared to experiment. $\alpha = 20deg\ Re = 4.2 * 10^6$

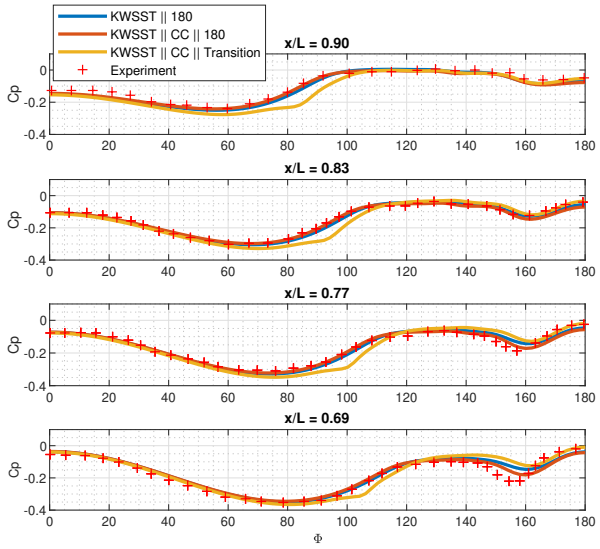

Figure 6.6 Surface pressure for coarse and fine mesh simulations compared to experiment experiment. $\alpha = 20deg\ Re = 4.2 * 10^6$

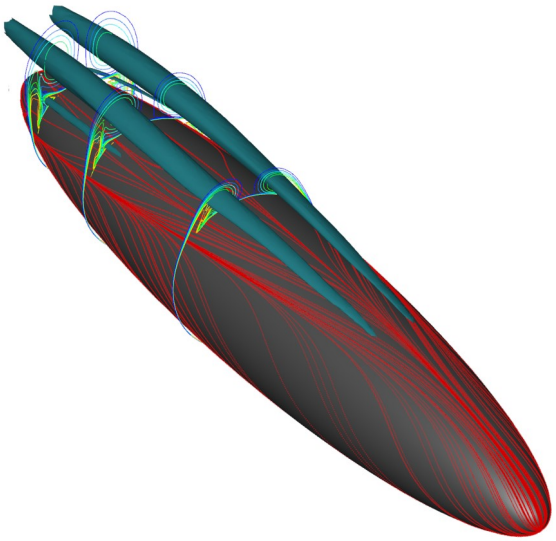

Figure 6.7 Reconstruction of free-stream structures. Iso-surfaces of Q-criteria are shown passing through slices of vorticity magnitude. $\alpha = 20deg\ Re = 4.2 * 10^6$

6.1.2. Transcient

Here the transient simulation results will be compared to that of the experiment. These results at four angles of attack are presented below. While the majority of these results compare quite nicely to experiments, there is a singular exception found at an angle of attack of 20 degrees that should be mentioned. At this angle of attack, the experimental results show that there is a strong secondary separation, yet the simulation was not able to reproduce this feature until an angle of attack of 22 degrees. It is believed that this discrepancy appears as a result of the simulation not properly modeling the transition regions between laminar and turbulent boundary layers. This historically has been an issue in turbulence modeling, with much effort being spent on efficiently modeling such transitions. Yet, given that the end goal of this research is to produce a ROM which can properly resemble forces for a 6-DOF model, a tolerance is allowed in this study for such discrepancies in surface pressures between the simulation and experiment.

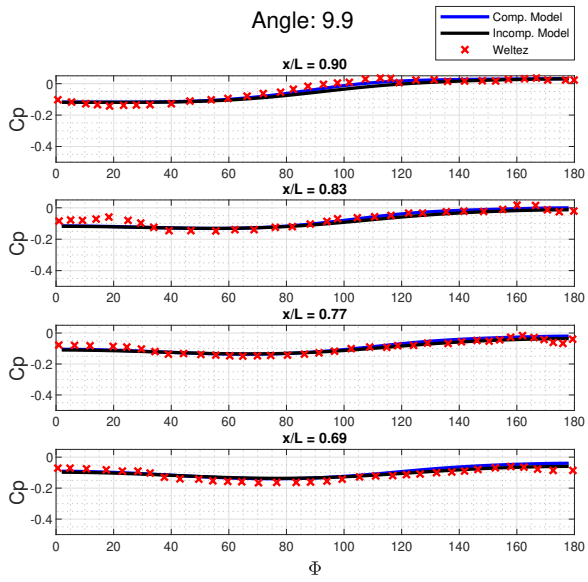

Figure 6.8 Surface pressure for compressible and incompressible simulations compared to experiment experiment. $\alpha = 9.9deg\ Re = 4.2 * 10^6$

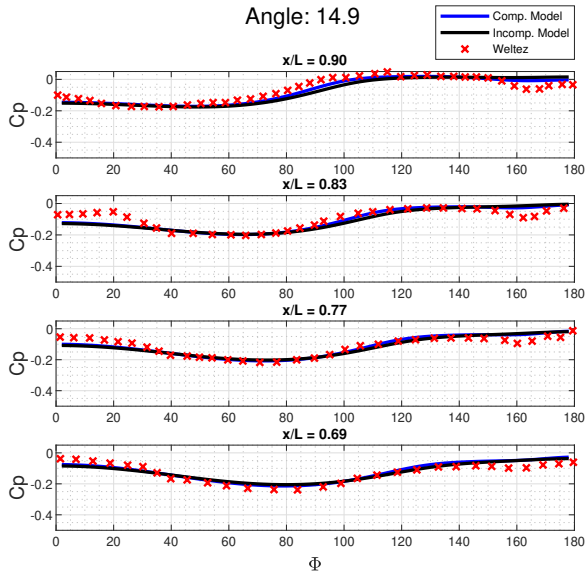

Figure 6.9 Surface pressure for compressible and incompressible simulations compared to experiment experiment. $\alpha = 14.9deg\ Re = 4.2 * 10^6$

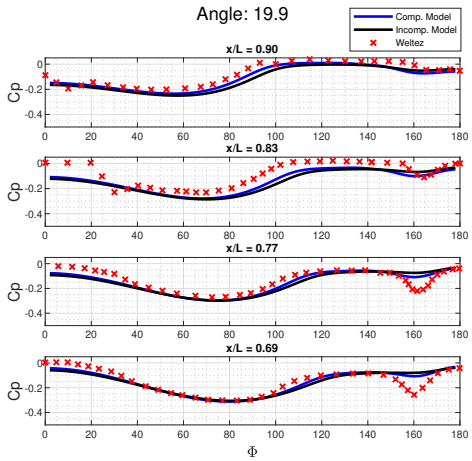

Figure 6.10 Surface pressure for compressible and incompressible simulations compared to experiment experiment. $\alpha = 19.9deg\ Re = 4.2 * 10^6$

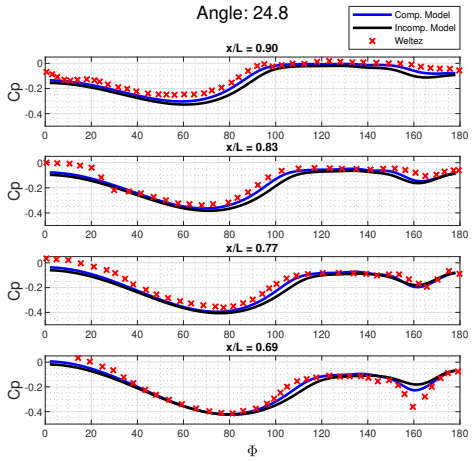

Figure 6.11 Surface pressure for compressible and incompressible simulations compared to experiment experiment. $\alpha = 24.8deg\ Re = 4.2 * 10^6$

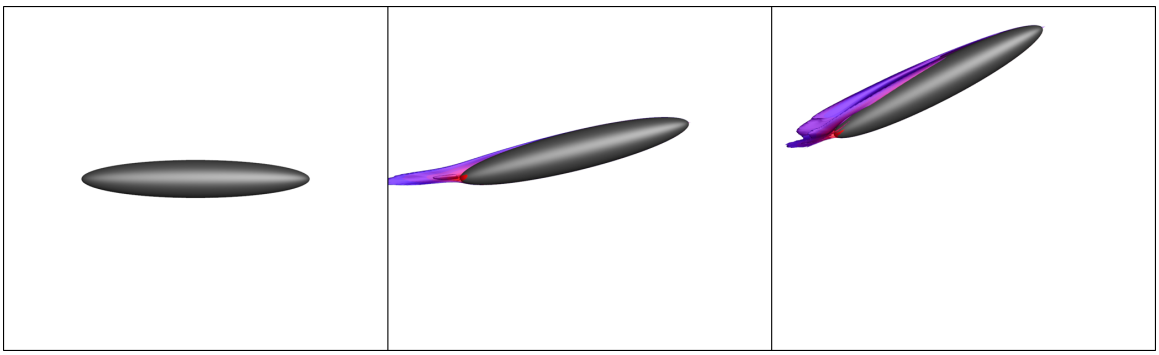

Figure 6.12 Three images of store under going pitch up motion. Iso-surfaces of vorticity magnitude colored by pressure.

6.2. Store Separation: Mach 0.8

The final simulation used in this study was a full store separation case at a Mach number of 0.8. The computational cost of running this simulation is provided in Table 6.2. Table 6.2 helps to illistrate the extreme difficulty in attempting to incorpate even RANS modeling into the store separation analysis. Even for the significantly idealized case of store separation considered in this study, computational time and expense begin to become impractical for store separation analysis outside of limited flight conditions.

Table 6.2

Summary of computational expense in running Mach 0.8 simulation

Parameter	**Cost**
Processors	20-E5-2697v4
Core	360-cores
Speed	2.3GHz
Run Time	168 hours

The motion of the store can be summarized through the four images shown in Figure 6.14. In the first image, at time 0.055 s, the store appears to be separating smoothly away from the fuselage. This observation is reinforced through observing the first 0.055 s of motion displayed in Figure 6.13. Figure 6.13 shows minimal change in pitch of the store during separation initially. This is because the pitching moment acting on the store over this time frame is extremely low. Yet, as is the case with many stores, the store used in this study is a neutrally stable body with the center of mass located in the exact center of the store. As such, the store's downward pitching motion initiates between the first and second image of Figure 6.14. From here it is observed that the pitching moment on the store has an expected exponential relationship with angle of attack. This relationship causes the noticeable unstable pitching of the store in the final two images of Figure 6.14.

It is of importance to note that the entirety of this motion can be traced back to the initial pitching moment acting on the store. This moment is caused by an acceleration of the flow behind the store's center line. This leads to an imbalance of surface pressures ultimately leading to the initial pitching moment.

In Figure 6.15, surface pressure contours of the store are provided. These contours will be used in the Reduced Order Modeling section of this report to draw comparison between model and simulation.

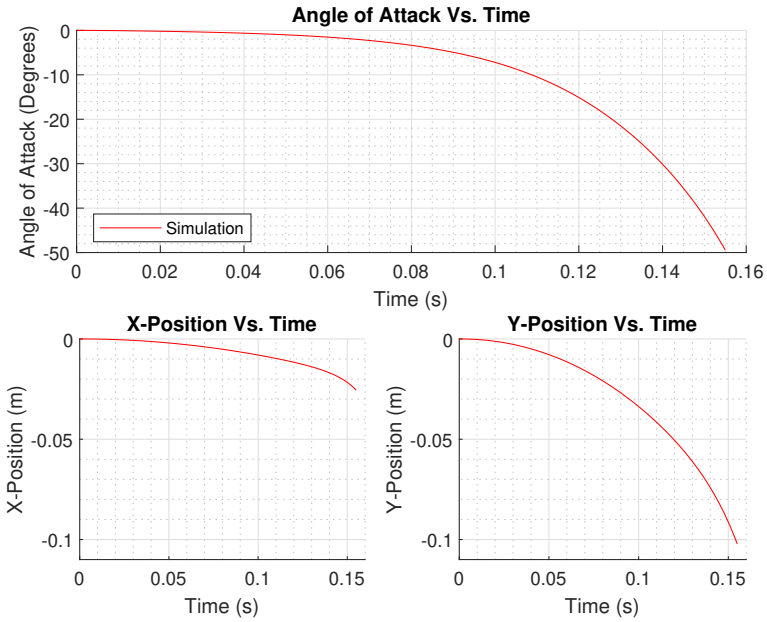

Figure 6.13 Time history of x-position, y-position, and α during simulation.

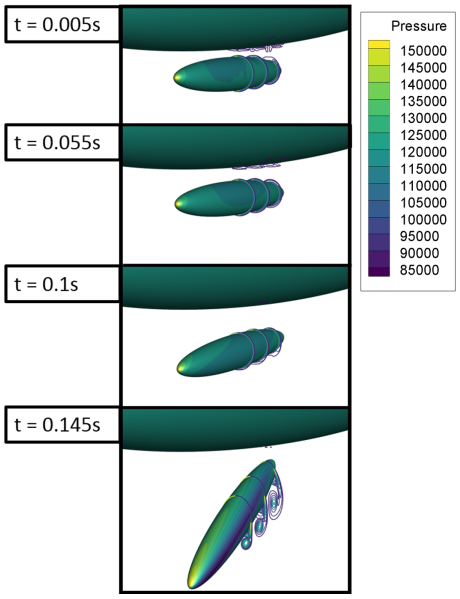

Figure 6.14 Four snapshots in time of store undergoing separation. Store is colored by pressure contours and three slices of vorticity magnitude are taken.

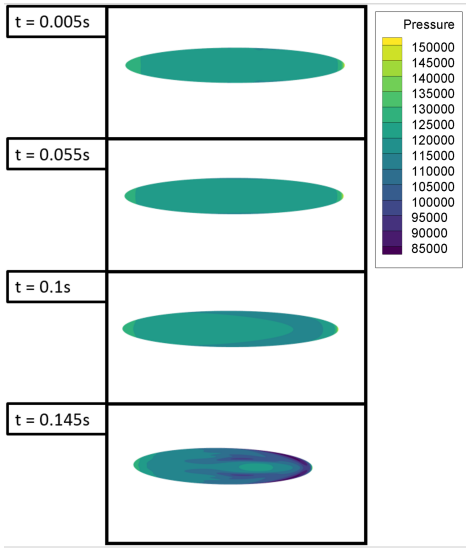

Figure 6.15 Four snapshots in time of store undergoing separation. Store is colored by pressure contours.

7. Reduced Order Model

In this section of the report, all modal analysis and ROM findings will be presented. The pitch up motion case will be analysed first and a comparison will be drawn between DMD and POD. The store separation case will then be analyzed and a complete ROM will be constructed and compared to the original CFD data-set.

7.1. Pitch Up: DMD vs. POD

With the results validated a modal analysis can now be completed. This analysis will consist of comparing the ability of POD and DMD to obtain modes which represent the surface and free stream structures of the flow field. This will be done through analyzing both surface pressures and a slice of vorticity magnitude taken at the 90% chord length of the store.

7.1.1. POD: Surface Pressures

After running the transient pitch up case for the store, 144 snapshots were taken and formed into a snapshot matrix. These snapshots consisted of surface pressure readings. From here the algorithm outlined in the Modal Analysis Methods section of this report was used to obtain modes. The first 12 singular values obtained through this algorithm were taken and plotted. By observing the trend of the singular values, we can see that the vast majority of the energy of the system is contained in just the first four modes. These four modes show the following trend. The first mode represents the pressure field for the vast majority of the store's motion, a fully attached flow field. For the vast majority of the store's motion, there is no primary or secondary separation. It is not until the much higher angles of attack that the flow actually begins to separate and form the primary and secondary vortex structures. The second mode shows the beginning of the formation of the primary separation regions. The third mode shows the fully formed primary separation and the beginning stages of secondary separation. Finally, the fourth modes includes both the fully formed primary and secondary separation on the store.

By using just these four modes, it is possible to re-project them back onto the original snapshot matrix and see how well they represent the original data-set. This

four mode subspace shows that not only are the original pressures modeled correctly, but also the original forces. As a final step, a comparison was made between keeping twelve modes and four modes for the ROM. These results show that there appears to be no significant advantage in tripling the subspace to increase accuracy.

One conclusion from this analysis is the simplicity in using POD to process a data-set into an extremely low-dimensional subspace. After pre-processing the data-set, all that was needed was SVD to obtain modes. The only additional step was a simple observation of the singular values. In just these three steps a well defined subspace was identified for the pitch up motion of the store. As mentioned earlier in this report, in order to have practiced mode-based-ROM's, they should be not only be quick to run but also reasonable to setup. A modal analysis of surface pressures for the pitch up case contributes significantly to the point that POD can be a very quick algorithm to obtain a well posed subspace.

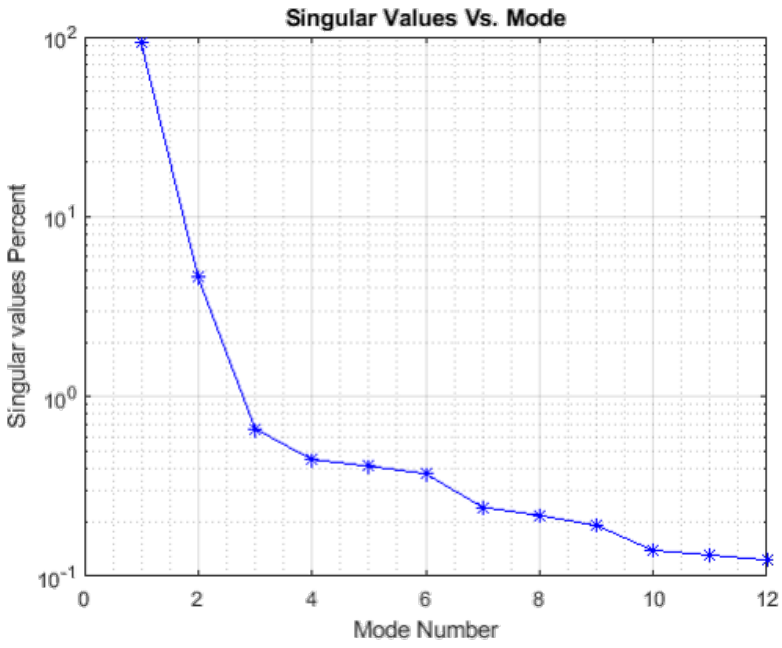

Figure 7.1 POD surface pressure singular values.

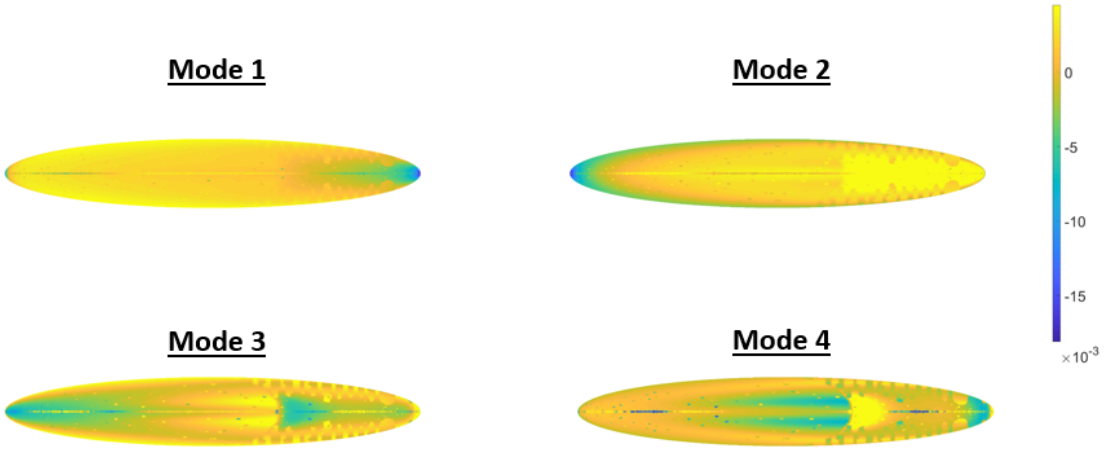

Figure 7.2 POD surface pressure first four modes.

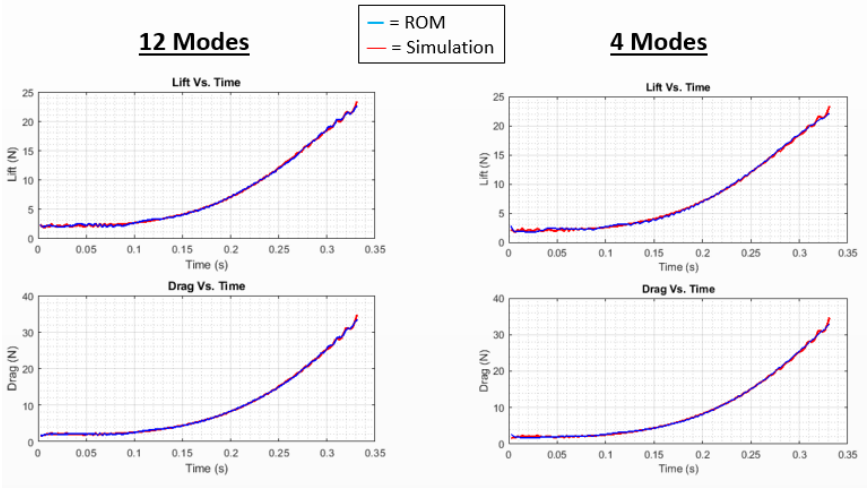

Figure 7.3 ROM force comparison between using 12 and 4 modes.

7.1.2. DMD: Surface Pressures

Here, the results for DMD on surface pressures are presented. The results show that many more modes are needed from DMD to accurately resolve the original system when compared to POD. While the modes from DMD are able to resolve the latter regime of the pitch up motion they are not able to accurately show the beginning stages. These results are consistent with what should be expected. DMD attempts to find time correlations which can be used to introduce frequency considerations into the results. This step works great when attempting to model fluid bodies with both high energy and strong time dynamics.

Yet, with the pitch up motion of the store there were not many frequency structures.

Rather, the system was dominated by structures with fixed growth rates. It is the result of looking for time correlations where there are none which leads to DMD modes that do not represent the system well. This is shown by the fact that not many of the DMD eigenvalues align with the unit circle on the complex field. The only modes out of the first twelve that do align with the unit circle are modes 9, 10, 11, and 12. These modes appear in complex conjugate pairs and appear with very small imaginary eigenvalue terms. This reaffirms the previous statement by showing that the modes which DMD finds to correlate well to the system are associated with very small frequency rates.

One potential counter argument to the statements made in this section is that this study only investigated an abnormally small subspace to replicate the data-set. This argument is based on the idea that if the subspace was allowed to grow, say by 200 modes, then it is possible that a better replication of the original data-set could be made with DMD than POD. The study will not attempt to counter the claim that a more exact representation could be made with a larger subspace. However, the issue with this claim is that it forgets that the objective of this work is to construct a ROM capable of running full store separation simulation as fast as possible on as few computational resources as possible. If the subspace is allowed to grow by too much, the computational cost of the ROM will begin to quickly balloon. As such, it is essential that the subspace identified be as small as possible.

These results should not be taken to mean that DMD is an inferior method to POD. The results simply show that, for the system that was observed in this study, POD is better suited to identify surface pressure structures.

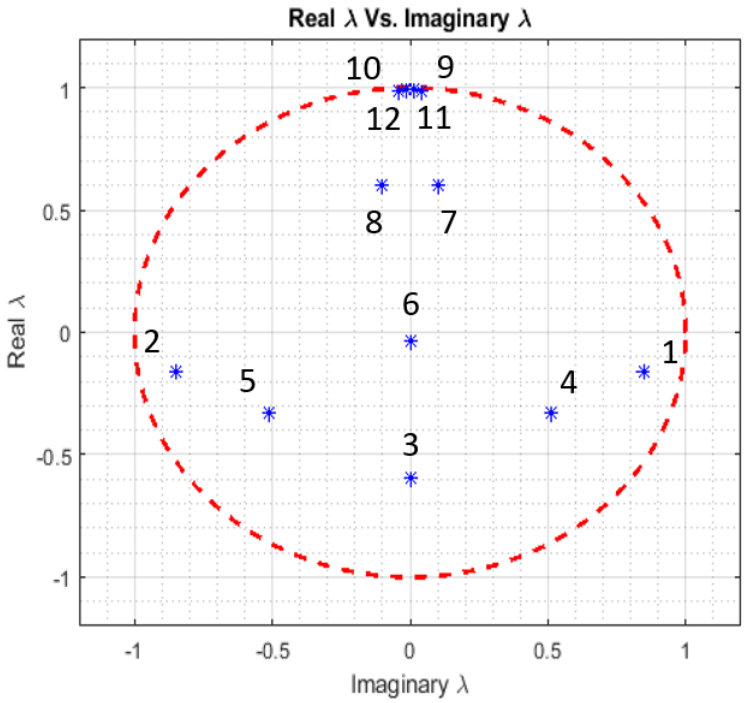

Figure 7.4 DMD eigenvalues.

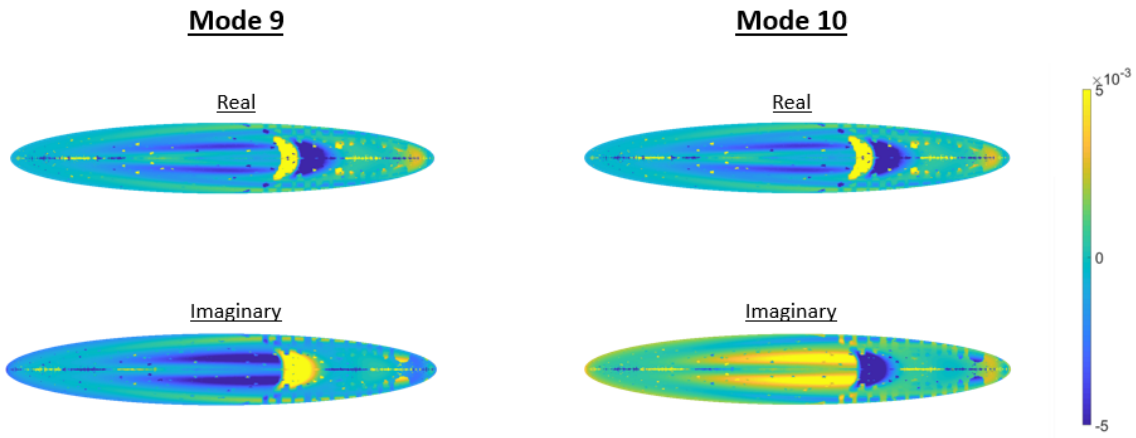

Figure 7.5 Real and imaginary modes 9 and 10.

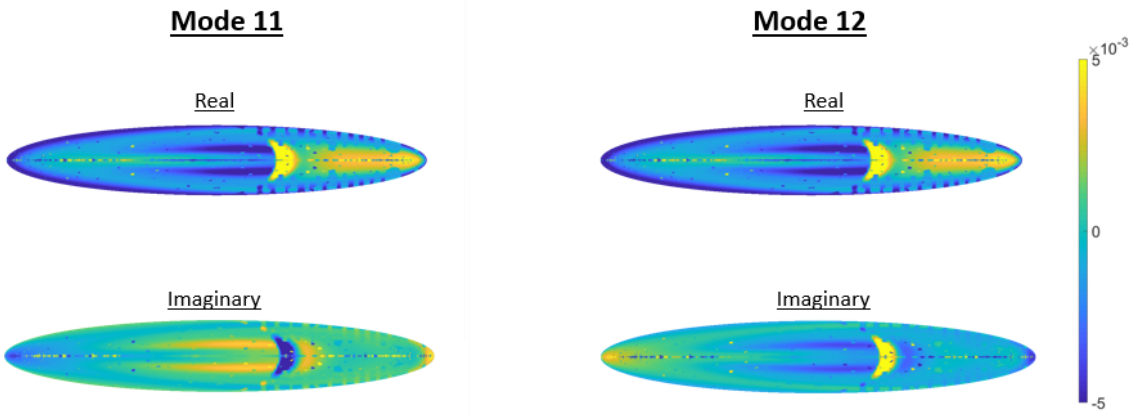

Figure 7.6 Real and imaginary modes 11 and 12.

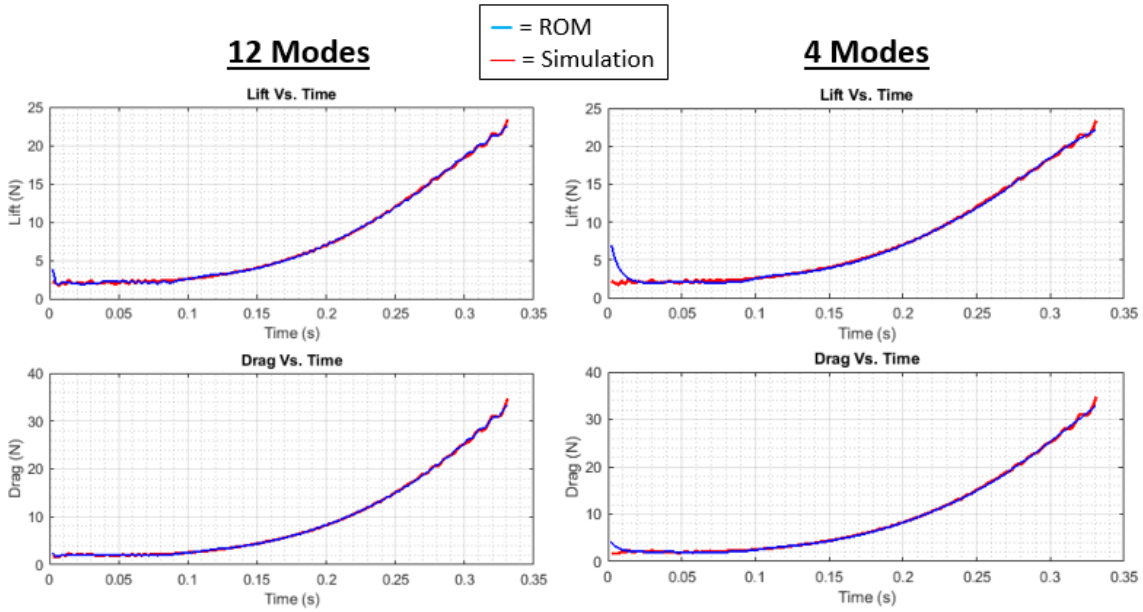

Figure 7.7 ROM force comparison between using 12 and 4 modes.

7.1.3. POD: Vorticity

When observing the capability of POD and DMD to identify free stream structures, a similar story is told as with the surface pressures. Once again, with a limited number of modes, the original data-set can be nicely reconstructed. With these results, only the first four modes will be reviewed in how they re-project back onto the snapshot matrix. The choice to only look at the first four modes becomes justified when looking at the singular values for this section. It is clear that the vast majority of the energy in the system is held

in these first four modes when compared to the singular values of the surface pressure case.

When looking at contours of the eigenfunction values for these modes, we see first that mode one is showing the mean flow around the store. Mode two shows the primary vortex structures. Mode three shows both the primary and secondary vortex structures and finally mode four attempts to show the intermediate locations of these vortex structures. By simply using these four images, a nice reconstruction of the flow field is produced at both low and high angles of attacks.

The findings of this section of the analysis show that not only can POD quickly find a representative subspace for surface pressures but also for the much more complicated free-stream structures. The ability to develop a subspace for free-stream structures was particularly in question due to the presence of large and much more common scalar gradients in the data-set matrix. Consider the image of the slice of vorticity. There is a region of extremely large gradients which exist between the inner and outer core of the primary vorticity.

Before this analysis, it was questioned how well POD would work in a space where large gradients are present. Remembering from the discussion in ‘Modal Analysis’, the modes which are acquired through POD can almost be taken as averages of energy contents of the data-set. One possibility was that the modes would simply smooth out all gradients in the complex flow field. However, these results show that they can in fact be resolved very efficiently.

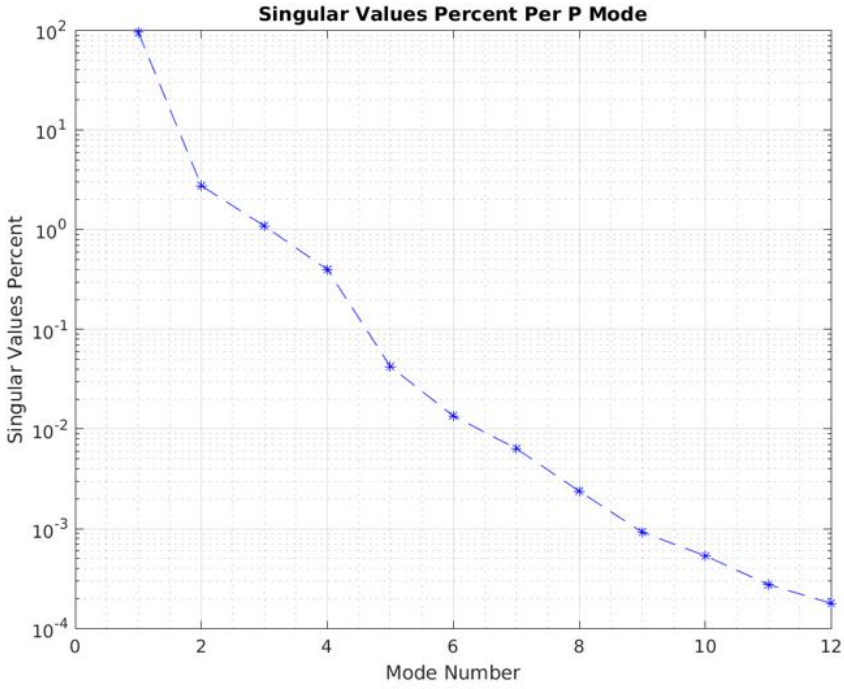

Figure 7.8 POD Singular Values for vorticity magnitude slice (POD). Plot only showing Singular Values for first twelve modes.

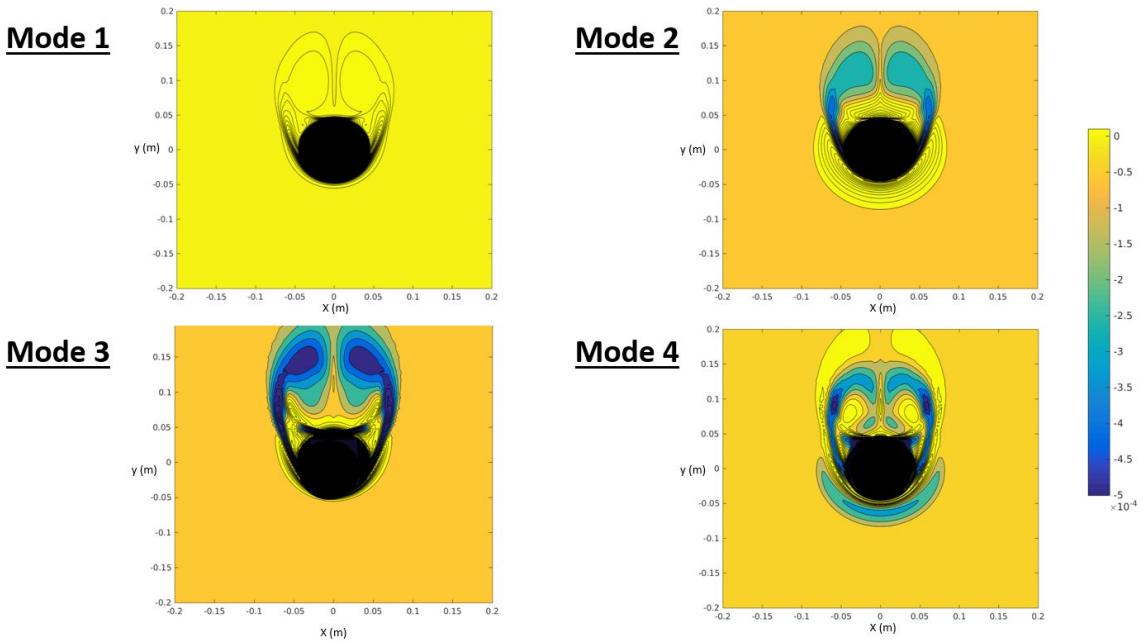

Figure 7.9 First four modes for POD. Contours are in-terms of eigenfunctions and are unit-less.

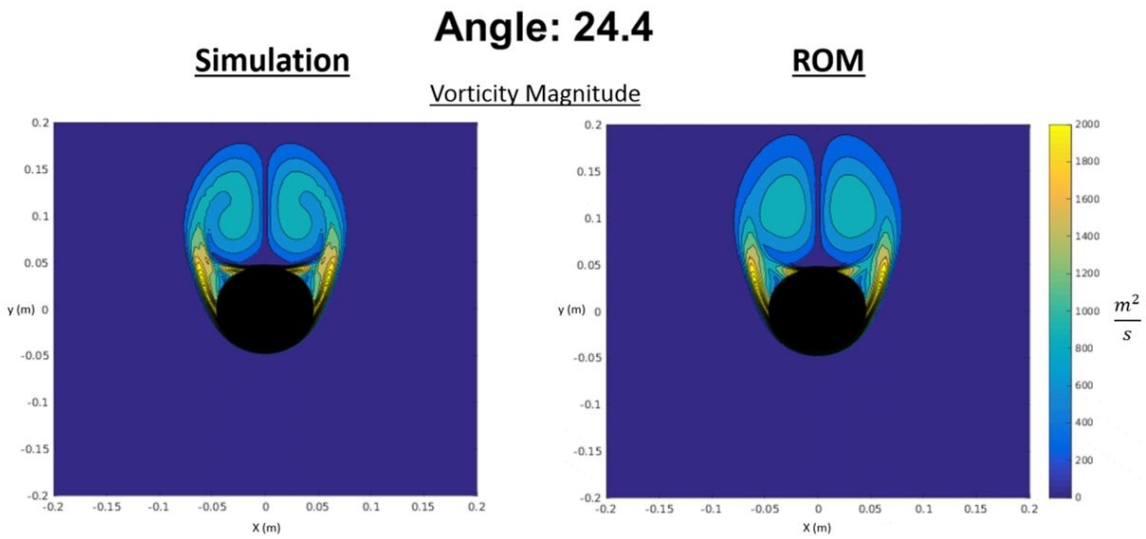

Figure 7.10 Comparison between ROM and simulation results.

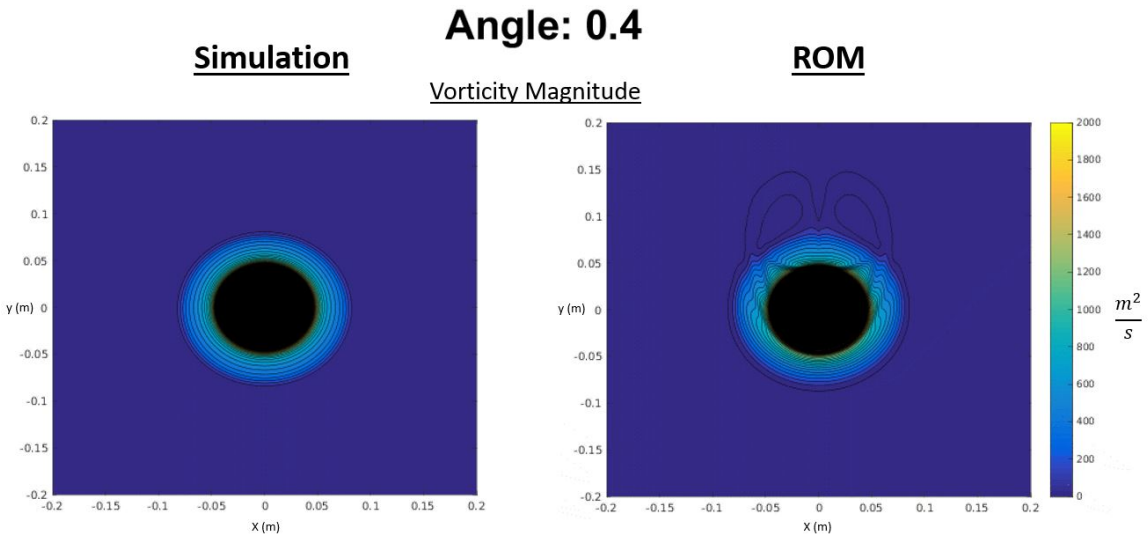

Figure 7.11 Comparison between ROM and simulation results.

7.1.4. DMD: Vorticity

When the DMD algorithm was used to find the modes for the system it became much more difficult to make meaningful correlations to the known structures. While, unlike for surface pressures, DMD was able to find modes which aligned nicely on the unit circle when plotting contours of the modes it became clear that the desired structures were not being resolved. An attempt was still made to re-project four modes back onto the original system. However, while these results are still presented below they show that a much larger subspace is needed to accurately represent the original snapshot matrix.

Just as with the surface pressure results, the inclusion of frequency terms in the DMD algorithm results in an erroneous representation of the known structures of the flow field. Mode one of the DMD best summarizes these results. Instead of representing the modes as they appear in space, DMD attempts to produce the structures as they move in time. As such the DMD algorithm attempted to locate elements in the original data-set which contained a high amount of energy. After finding these element energy states the algorithm then attempted to replicate the frequency in which they were changing. This method of mode finding would have work excellently if the vortices where to have been shedding at a fixed frequency.

However, the vortices which form never shed off the body and as such there was no such frequency associated with their motion. Their motion is much better associated with fixed/decay growth rates rather than a frequency. As such, it becomes much easier to identify these structures in space rather than time.

In future work to this study, there may be scenarios in which DMD's algorithm my work better. One such scenario which might have allowed DMD to be better taken advantage of is the case of increasing the maximum pitch of the store. At higher pitch these primary vortices will become asymmetric and will oscillate as a result of global instability of the flow field. This global instability may be better resolved by DMD. However, this condition was out of the scope of this study.

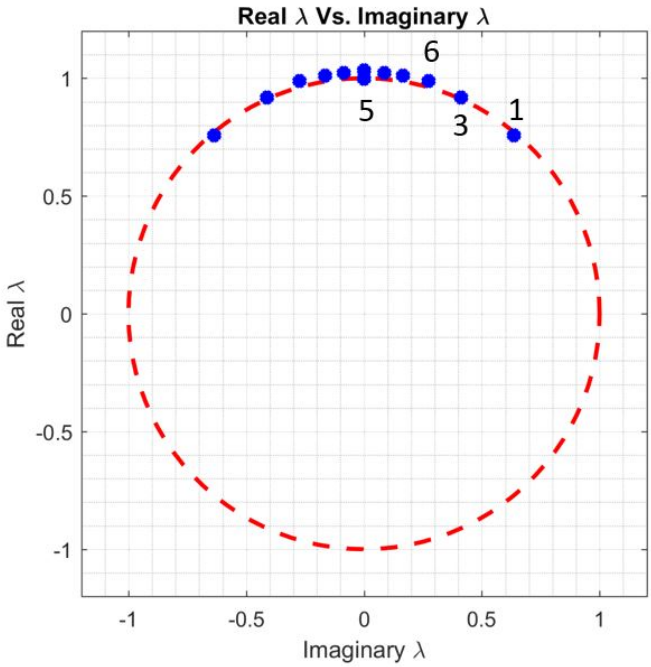

Figure 7.12 Eigenvalues for vorticity magnitude slice (DMD). Modes 1, 3, 5, and 6 are called out. They are the four modes which were used to reconstruct the snapshot matrix.

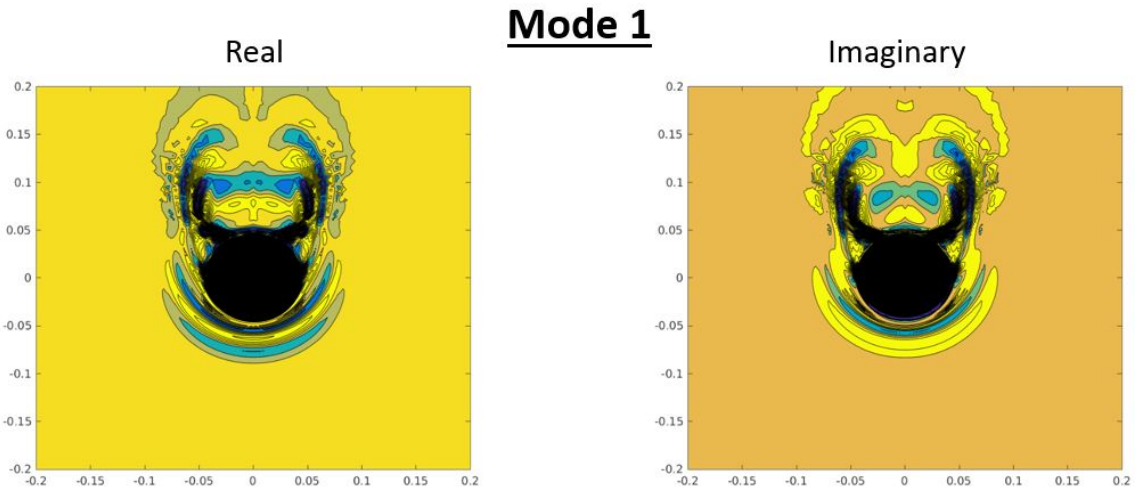

Figure 7.13 First mode for DMD. Only the first mode is presented as all other modes show a very similar trend of not representing physical structures. Contours are in terms of eigenfunctions and are unit-less.

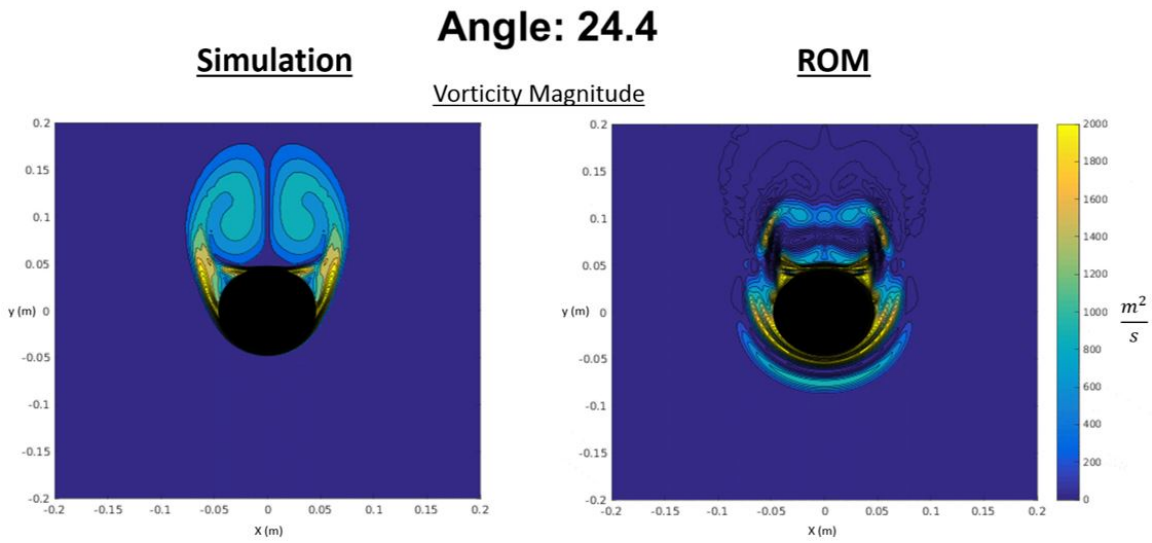

Figure 7.14 Comparison between ROM and simulation results at 24.4 α.

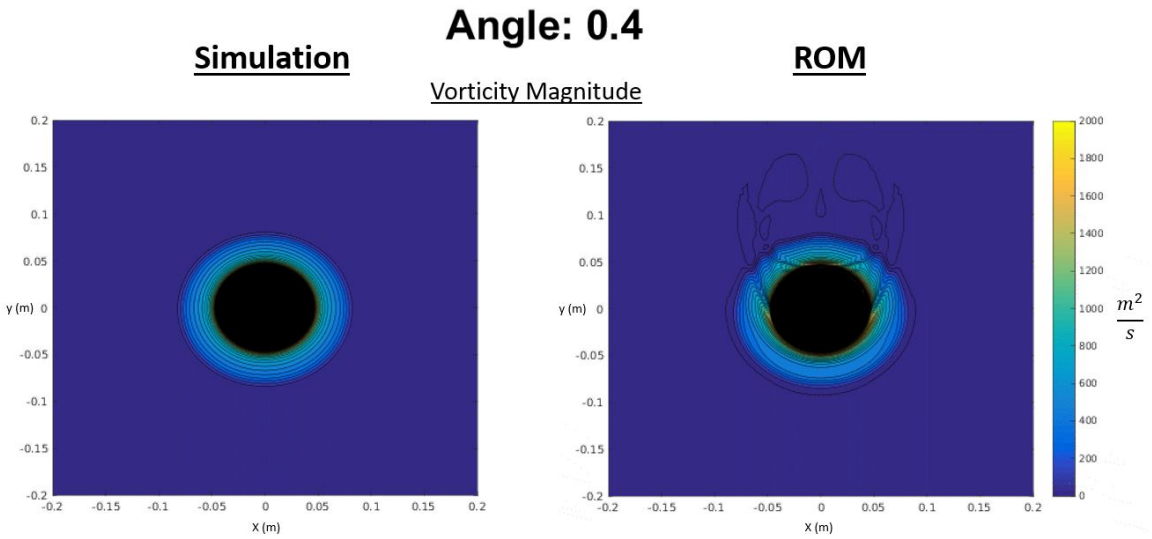

Figure 7.15 Comparison between ROM and simulation results at 0.4 α.

7.2. ROM vs. Simulation: Mach 0.8

Up to this point in the report, much effort has been spent on reviewing how to develop a low dimensional subspace from a high dimensional data-set. In this section of the report, further steps will be taken to present the actual application of a new found subspace to a data-driven interpolation ROM. The first step for constructing the desired ROM for Mach 0.8 was to derive a representative subspace. The information found in the Pitch Up ROM sections of this report point to the logic that POD is an extremely efficient algorithm for converting to a subspace. As such, only POD was used to develop

the desired subspace. After formulating a snapshot matrix from the Mach 0.8 simulation, a POD modal analysis was completed for both free stream and surface pressure structures.

7.2.1. Singular Values

After observing Figure 7.16, which shows singular values for the store's surface pressures, it is observed that there are three main groupings of singular values. The first grouping shows an exponential decrease in values between modes 1 and 4. The energy levels then flat line between modes 5 and 7 before sharply decreasing around mode 8. Being able to retain as much of this energy as possible is essential in reconstructing the ROM. As will be shown later, in order to properly model the store's trajectory a precise aerodynamic model will need to be constructed. Even small differences in loads early on in the store's motion will ultimately cause a very different trajectory. As such, it was determined that two ROMs would be constructed; one based on a subspace of 4 modes and another with 8 modes.

When observing the singular values for the the free-stream vorticity magnitude, a very similar trend is followed between Figures 7.17 and 7.16. Once again, there is an exponential decay in the singular values from modes 1 to 4. From here, two notes of importance need to be discussed for the free-stream ROM. First, it should be noted that modeling of free-stream structures of the flow field comes at great computational cost. Whereas with surface pressures which have a total spatial domain of 53,642 nodes, the free-stream analysis instead included 5,364,200 nodes. This greatly increased the matrix sizes and with it computational cost. This leads to the second note of importance. For the case of this study, the object of constructing a free-stream ROM was to simply mimic the free-stream structures of the flow field in both phase and magnitude with reasonable accuracy. Free-stream structures being off by small margins would ultimately not affect the stores trajectory. As such, only one ROM was constructed for the free-stream using the first four modes.

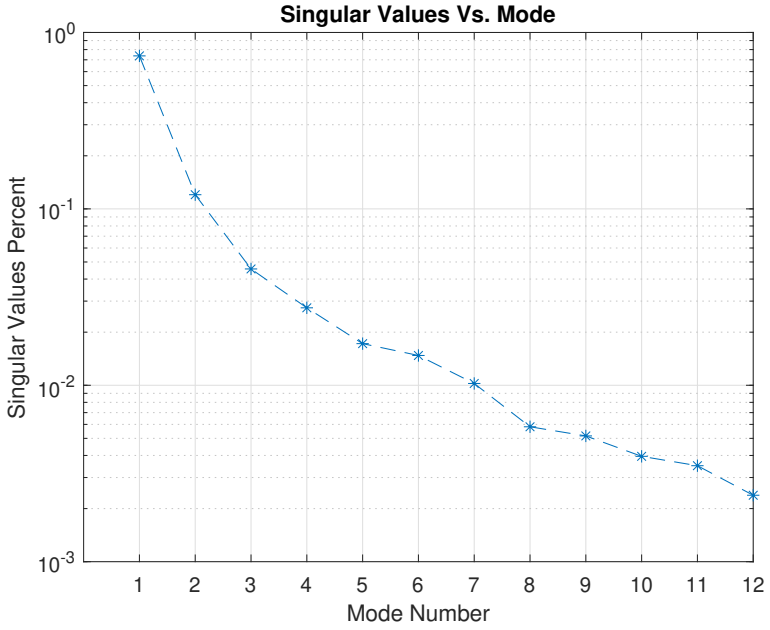

Figure 7.16 Singular Values for surface pressure (POD).

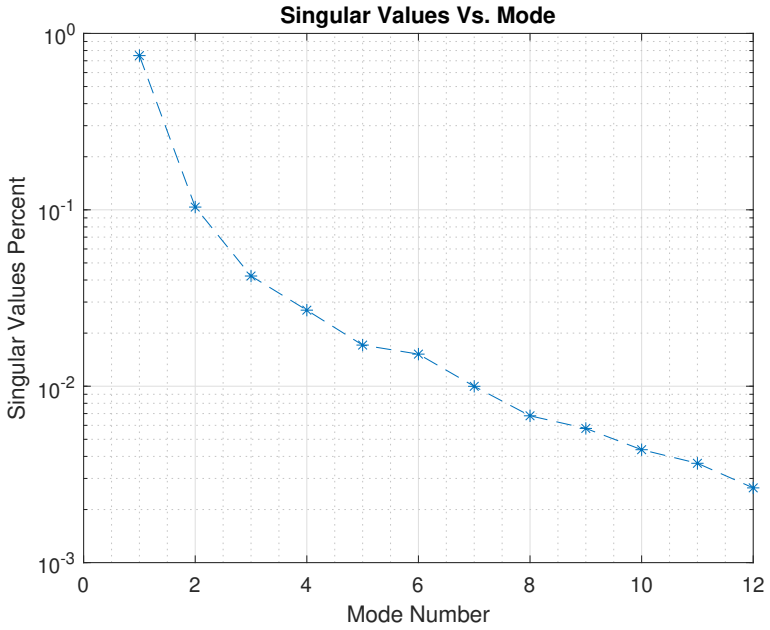

Figure 7.17 Singular Values for vorticity magnitude (POD).

7.2.2. Modal Analysis

The first four modes found using POD on surface pressures are presented in Figures 7.19 and 7.20. The first four modes found in this case are very similar to that of the pitch up motion cases. The first mode appears to provide an averaged value to the stores

surface pressures. Mode 2 shows the influence of the primary separation while mode 3 shows both primary and secondary separation. Finally, mode 4 once again attempts to model the separation traveling across the body.

While not exactly the same, the conclusion that the modal analysis appears to derive similar surface pressure modes with both an isolated store and a store under the influence of a fuselage is important. The first significant conclusion from this observation is that the store's motion undergoing separation is dominated by the same structures as an isolated store. Initially, the fuselage-store interaction influences a perturbation on the store. However, from here the store's natural fluid structures which develop begin to dominate the aerodynamic forces on the body. This conclusion lends credit to the possibility of developing a ROM based on an isolated store's motion. This ROM could potentially then be given a perturbation to mimic the initial fuselage store interaction. However, for the time being this topic is outside the scope of this study, as will be addressed in the Future Recommendations section of this report.

The free-stream modes used in this study can be found in Figure 7.18. Mode 1 was excluded from Figure 7.18 as no free-stream structures were present. Just as the surface pressure modal analysis led to a similar comparison to the pitch up motion, so too does the free-stream analysis. Once again, with a very limited subspace, the full data-set is closely captured.

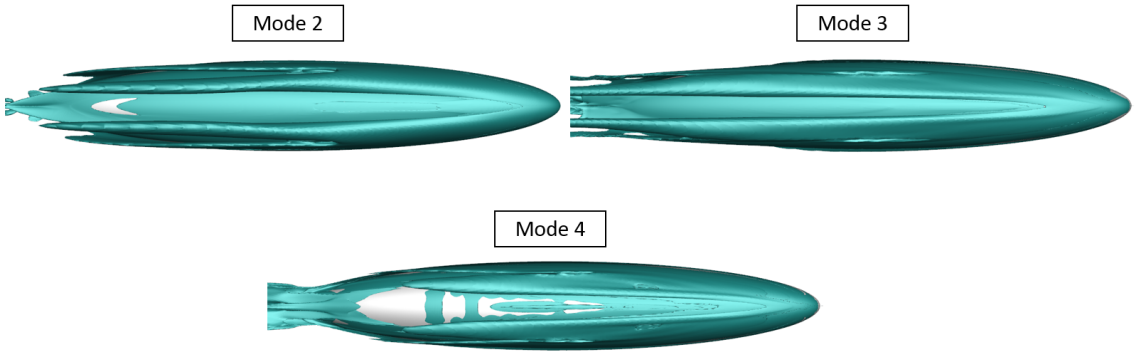

Figure 7.18 Iso-surfaces of POD free-stream for modes 2 through 4. Bottom up view of store.

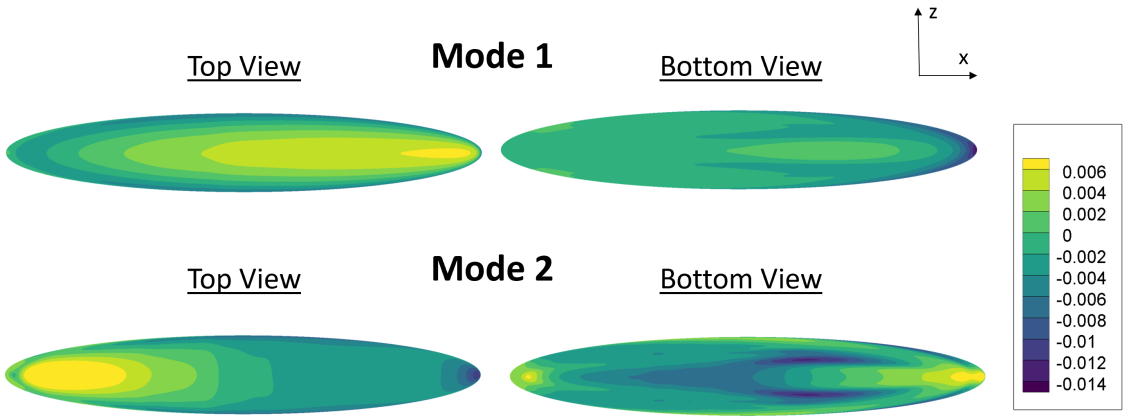

Figure 7.19 Contours of POD surface pressure for modes 1 and 2. Includes bottom and top views of store.

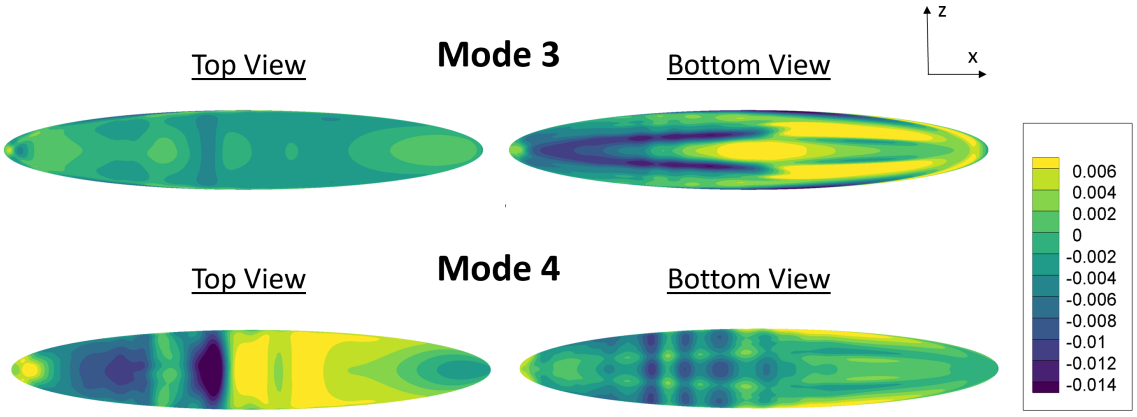

Figure 7.20 Contours of POD surface pressure for modes 3 and 4. Includes bottom and top views of store.

7.2.3. ROM Comparison

The next step of the ROM study was to simply project the modes back onto the original data-set and see how well they capture the lift and drag forces on the store. The results of this first step can be found in Figures 7.21 and 7.22. These Figures show that, while the 4 mode ROM does a good job of capturing the forces, there still remains seemingly minor discrepancies between simulation and ROM. These seemingly minor discrepancies end up becoming very important when attempting to predict trajectories of the store. As such, it was important to expand the working subspace to 8 modes. By doubling the subspace, a much better representation of the forces can be made and

thereby a much more accurate trajectory prediction.

To construct the mode based ROM, an interpolation scheme was incorporated. As stated in the Modal Analysis section, the first stage of this process is to undergo an expansion of terms which could be used to create a function for the time coefficients. Equation 19 is restated below:

$$a_t = F(\alpha, \dot{q}, U_\infty, \rho_\infty, T_\infty ...) \tag{78}$$

By recognizing that the data-set currently being used is limited to a single flight condition, a vast reduction of terms can be assumed.

$$a_t = F(\alpha, q, h) \tag{79}$$

In Equation 79, h is the stores distance from the fuselage. A further reduction of terms can be made by considering which terms most dominate the stores motion. By comparing the change in magnitude for each of these variables, it becomes clear that the most dominant variable to the stores motion is α. As such, the interpolation model will be based strictly on α.

$$a_t = F(\alpha) \tag{80}$$

Given that, after the projection, a series of a_t and α data exist, a linear interpolation model can be constructed. While higher order interpolation schemes could have been used, the idea was to for now keep the development of this model as simple as possible while still retaining high accuracy. If a higher order scheme was needed, then a new model could quickly be derived.

The function described in Equation 80 was used with the first 8 surface pressure modes and the first 4 free-stream modes to construct the ROM used to predict the store's trajectory. This ROM allowed the study to compute the full flow field about the store at very little computational cost. The cost of these models are outlined in Table 7.1.

After constructing a series of functions for a_t, a 3-DOF model was developed in MATLAB. This 3-DOF model was then coupled with the newly developed ROM. As shown in Table 7.1, these newly constructed models operate at extremely low

computational power compared to that of the full simulation. Instead of taking a week to simulate 0.155 seconds of simulation time on hundreds of cores, the recently constructed ROMs take mere seconds on a single, even slower core.

However, running the ROMs at low computational cost was only the first requirement of the study. The study also needed to show that the ROM could operate accurately within the data-set. Unfortunately, the results shown in Figure 7.25 show that the 4-mode based ROM was not able to accurately model the store's trajectory. While close, small discrepancies in surface pressures result in very different x-position, y-position, and α values by the end of the run. However, by expanding the subspace to 8 modes, the ROM was able to accurately model the trajectory of the store. An additional note of importance is that the ROM was also able to make accurate predictions of the trajectory of the store outside of the training data-set limit of 0 s to 0.145 s.

Table 7.1

Summary of computational expense in running both full simulation and 4/8 mode ROMS at Mach 0.8

	Full Simulation	**4-Mode ROM**	**8-Mode ROM**
Processors	20-E5-2697v4	1-E5-2620	1-E5-2620
Core	360-cores	1-core	1-core
Speed	2.3GHz	2.0GHz	2.0GHz
Run Time	168 hours	9.5 seconds	15.3 seconds

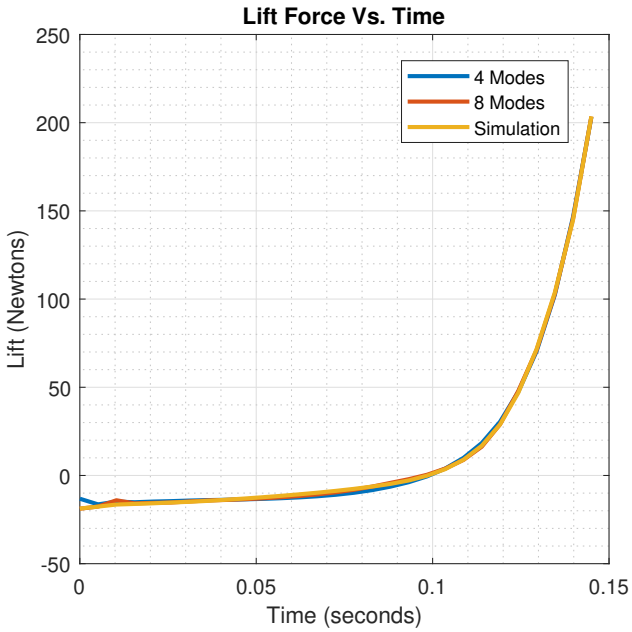

Figure 7.21 Lift comparison between ROM and simulation results with 4 and 8 modes.

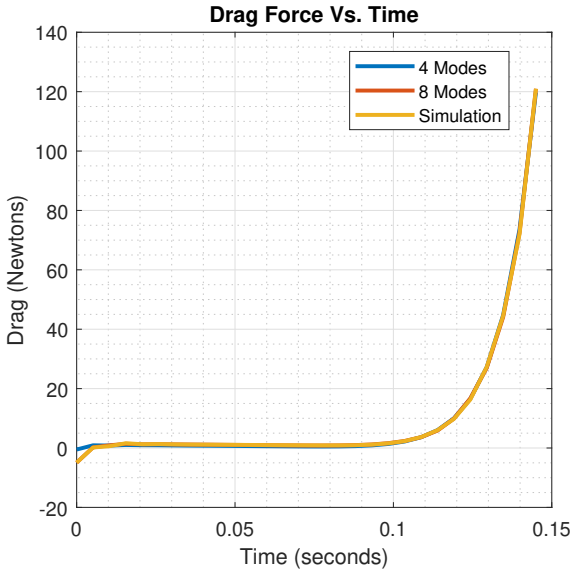

Figure 7.22 Drag comparison between ROM and simulation results with 4 and 8 modes.

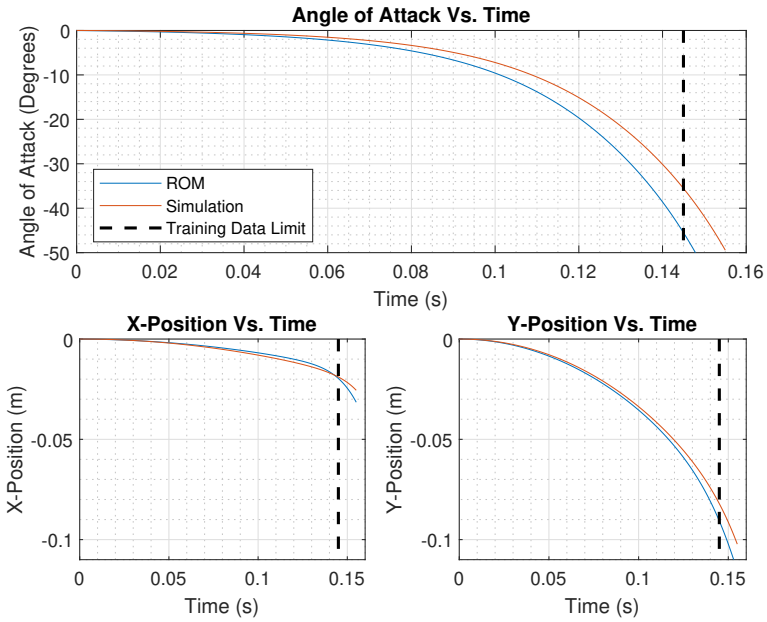

Figure 7.23 Comparison between ROM and simulation results with 4 modes.

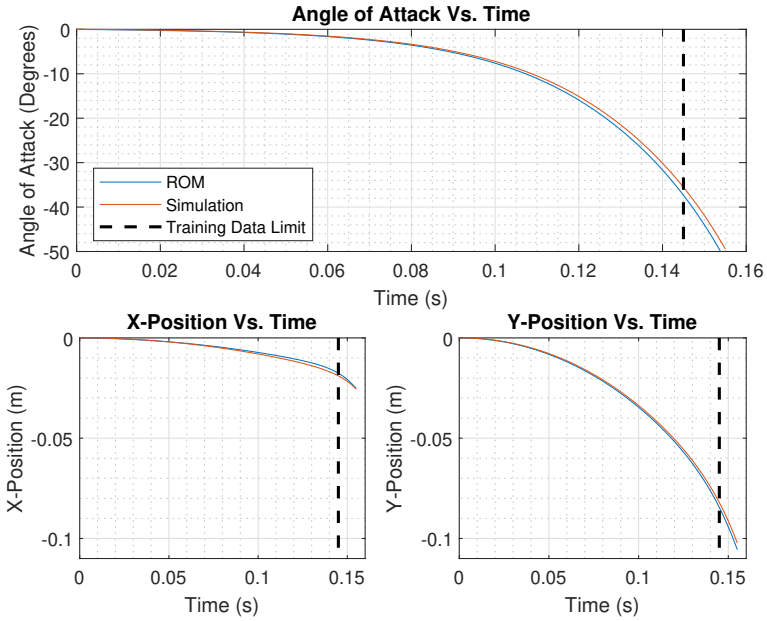

Figure 7.24 Comparison between ROM and simulation results with 8 modes.

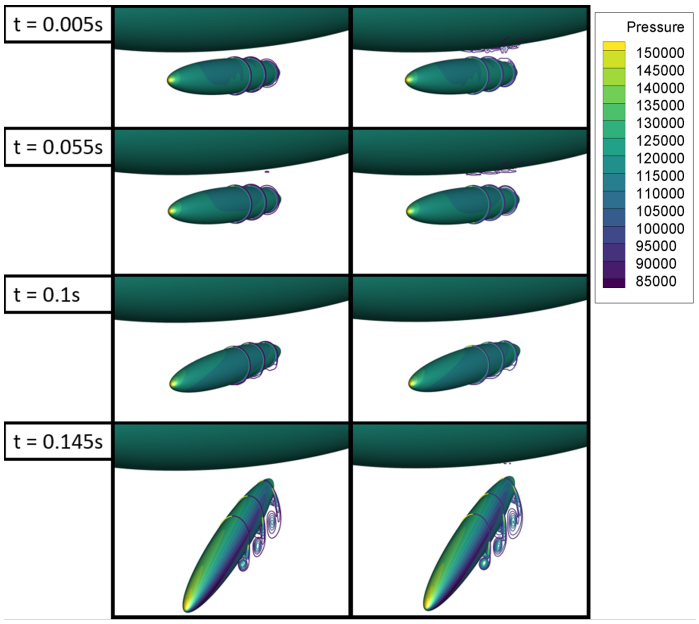

Figure 7.25 ROM (left) and simulation (right) comparison. Surface pressures reconstructed with 8 modes and free stream was reconstructed with 4 modes.

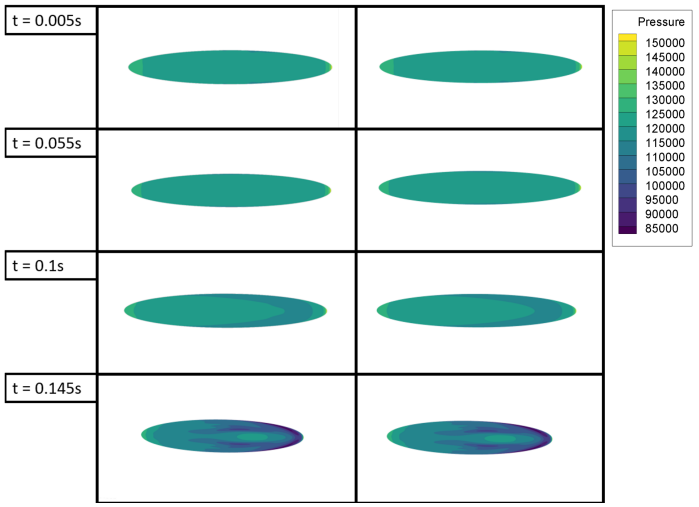

Figure 7.26 ROM (left) and simulation (right) comparison. Surface pressures reconstructed with 8 modes.

8. Conclusions and Future Recommendations

The first goal for this study was to compare POD and DMD to identify the better method for moving to a well defined subspace. The study found that the best method to use in identifying this subspace was POD. POD showed an incredible ability to quickly reduced large sets of data down into their fundamental components. Further more, the study also found that POD has an excellent capability to reduce the order of the system of interest. Not only was POD able to identify modes which identified leading structures of the flow, POD also was able to reduce the total system of 144 images down to simply 4 modes. This results in a 97% reduction in data. This should not be taken to mean POD will always operate better than DMD. As stated in the modal analysis methods section of this report, the capabilities of these methods to resolve structures that dominate a system comes down to the structures themselves. The structures that are desired to be resolved in this study are best associated with spatial correlations and not well defined with time correlations. This makes the problem of identifying structures of the flow field around a store very well suited for POD, but not well suited for DMD.

In attempting to show that this subspace could be used to construct a ROM for accurate trajectory predictions, an important series of conclusions was made. First, the study was able to identify a strong correlation between modes found in the pitch up and store separation cases. This correlation points to the possibility that an appropriate model for store separation could be constructed completely independent of obtaining fuselage-store interaction data. Yet such a ROM, while potentially efficient to construct, would be limited in application. While the results of this study show that, for this specific store separation case, the store motion could be captured by such a ROM, this is not true for all cases. Often, stores will fail to separate from their aircraft's boundary layer. In these cases, a ROM would potentially operate very poorly.

Another important conclusion is that it is possible to construct a ROM for store separation which both accurately models trajectories (Figure 7.24) and runs orders of magnitude faster than the original simulation (Table 7.1). Additionally, it was shown

that this model was able to operate accurately even when operating outside of the training data-set. These results indicate, that given a finite number of data points, it is feasible that a ROM could be constructed to operate across an entire flight profile for an aircraft.

With limitations to time and computational resources many topics which were of interest to this study ultimately had to be reserved for further work. A list of these topics is presented below.

- Investigate capabilities of POD and DMD in resolving moving shocks
- Investigate capabilities of POD and DMD in reconstructing asymmetric flow field (vortex shedding)
- Develop controller to assist in initial separation
- Develop ROM for an isolated store based on α and reduced frequency
- Validate that this ROM can operate outside of the original data-set
- Use this validated ROM to construct controller which can be used to assist in store separation

REFERENCES

Brunton, S. L., & Kutz, J. N. (2019). *Data-driven science and engineering: Machine learning, dynamical systems, and control*. Cambridge University Press, London U.K.

Cenko, A. (2010). *Store separation lessons learned during the last 30 years* (Tech. Rep.). Naval Air Systems Command, Patuxent River, MD.

Cenko, A., Richardson, P., Talbot, M., Loezos, S., Chaddock, D., & Piranian, A. (1996). Integrated t&e approach to store separation-dim past, exciting future. In *Icas proceedings* (Vol. 20, pp. 541–551).

Cenko, A., & Tinoco, E. (1979). Pan air-weapons, carriage and separation. *Air Force Flight Dynamics Labs-TR-79-3142*.

Cho, H.-K., Kang, C.-H., Jang, Y.-I., Lee, S.-H., & Kim, K.-Y. (2010). Store separation analysis of a fighter aircraft's external fuel tank. *International Journal of Aeronautical and Space Sciences*, *11*(4), 345–350.

Imperial War Museums. (2014). *In what other ways did aerial warfare develop?* British Army. Retrieved from https://www.iwm.org.uk/

Iqbal, M., & Thomas, F. (2007). Coherent structure in a turbulent jet via a vector implementation of the proper orthogonal decomposition. *Journal of Fluid Mechanics*, *571*, 281–326.

Israeli Computational Fluid Dynamics Center. (2010). *Cfd simulation of store separation from a fighter aircraft.* Retrieved from https://www.iscfdc.co.il/?q=media-gallery-storeseparation

Jolliffe, I. T. (2002). Springer series in statistics. *Principal component analysis*, *29*.

Lengani, D., Simoni, D., Ubaldi, M., Zunino, P., & Bertini, F. (2017). Experimental investigation on the time–space evolution of a laminar separation bubble by proper orthogonal decomposition and dynamic mode decomposition. *Journal of Turbomachinery*, *139*(3).

Liberge, E., & Hamdouni, A. (2010). Reduced order modelling method via proper orthogonal decomposition (pod) for flow around an oscillating cylinder. *Journal of fluids and structures*, *26*(2), 292–311.

Lumley, J. L. (1981). Coherent structures in turbulence. In *Transition and turbulence* (pp. 215–242). Elsevier.

Mohammadi, A., & Raisee, M. (2019). Stochastic field representation using bi-fidelity combination of proper orthogonal decomposition and kriging. *Computer Methods in Applied Mechanics and Engineering*, *357*, 112589.

National Aerospace Laboratories. (2018). *Captive trajectory system.* Retrieved from https://www.nal.res.in/en/techniques/captive-trajectory-system

Noack, B. R., Morzynski, M., & Tadmor, G. (2011). *Reduced-order modelling for flow control* (Vol. 528). Springer Science & Business Media, Berlin, Germany.

Panagiotopoulos, E. E., & Kyparissis, S. D. (2010). Cfd transonic store separation trajectory predictions with comparison to wind tunnel investigations. *International Journal of Engineering*, *3*(6), 538–553.

Paul, S., & Chang, J. (2017). Design and parametric study of the magnetic sensor for position detection in linear motor based on nonlinear parametric model order reduction. *Sensors*, *17*(7), 1543.

Pearson, K. (1901). On lines and planes of closest fit to systems of points in space. *The London, Edinburgh, and Dublin Philosophical Magazine and Journal of Science*, *2*(11), 559–572.

Pope, S. B. (2001). *Turbulent flows*. Institute of Physics Publishing, London.

Ramakrishnan, S., & Scheidegger, T. (2016). Overset Meshing in ANSYS Fluent. In *Ansys, 13th overset grid symposium, new york city.*

Schmid, P. J., & Sesterhenn, J. L. (2008). Decomposition mode decomposition of numerical and experimental data. *Bull. Amer. Phys. Soc*.

Spalart, P., & Allmaras, S. (1992). A one-equation turbulence model for aerodynamic flows. In *30th aerospace sciences meeting and exhibit* (p. 439).

Wetzel, T. (1998). Unsteady crossflow separation location measurements on a maneuvering 6: 1 prolate spheroid. *AIAA journal*, *36*(11), 2063–2071.

White, F. M., & Corfield, I. (2006). *Viscous fluid flow* (Vol. 3). McGraw-Hill, New York City.

Zikanov, O. (2019). *Essential computational fluid dynamics*. John Wiley & Sons, New York City.